Aqueous geochemical and microbial variation across discrete depth intervals in a peridotite aquifer assessed using a packer system in the Samail Ophiolite, Oman

Daniel Nothaft[1,1], Alexis S Templeton[2,2], Eric Boyd[3,3], Juerg Matter[4,4], Martin Stute[5,5], and Amelia N Paukert Vankeuren[6,6]

[1]University of Colorado - Boulder
[2]University of Colorado Boulder
[3]Montan State University
[4]University of Southampton
[5]Columbia University
[6]Sacramento State University

January 20, 2023

Abstract

The potential for molecular hydrogen (H-OH^- groundwaters bearing up to 4.05 μmol[?]L^{-1} H_2 , 3.81 μmol[?]L^{-1} methane (CH_4) and 946 μmol[?]L^{-1} sulfate (SO_4^{2-}) revealed an ecosystem dominated by Bacteria affiliated with the class Thermodesulfovibrionia, a group of chemolithoheterotrophs supported by H_2 oxidation coupled to SO_4^{2-} reduction. In shallower, oxidized Mg^{2+}-HCO_3^- groundwaters, aerobic and denitrifying heterotrophs were relatively more abundant. High $\delta^{13}C$ and δD of CH_4 (up to 23.9 CH_4 oxidation, particularly in Ca^{2+}-OH^- waters with evidence of mixing with Mg^{2+}-HCO_3^- waters. This study demonstrates the power of spatially resolving groundwaters to probe their distinct geochemical conditions and chemosynthetic communities. Such information will help improve predictions of where microbial activity in fractured rock ecosystems might occur, including beyond Earth.

Aqueous geochemical and microbial variation across discrete depth intervals in a peridotite aquifer assessed using a packer system in the Samail Ophiolite, Oman

Daniel B. Nothaft[1*], Alexis S. Templeton[1], Eric S. Boyd[2], Juerg M. Matter[3], Martin Stute[45], Amelia N. Paukert Vankeuren[6], The Oman Drilling Project Science Team

[1]Department of Geological Sciences, University of Colorado, Boulder, CO, USA
[2]Department of Microbiology & Immunology, Montana State University, Bozeman, MT
[3]National Oceanography Centre, University of Southampton, Southampton, UK
[4]Barnard College, New York, NY, USA
[5]Lamont-Doherty Earth Observatory, Columbia University, Palisades, NY, USA
[6]California State University, Sacramento, Sacramento, CA, USA

Key Points:

- Packers were used to sample groundwaters from discrete peridotite aquifers.
- The discrete aquifers contained waters with distinct chemical compositions and microbial communities.
- Chemolithoheterotrophic sulfate reduction was a dominant metabolic strategy inferred from 16S rRNA gene homology.

[*]Current address: Department of Chemical and Biomolecular Engineering, University of Pennsylvania 220 S. 33rd Street Philadelphia, PA 19104 USA

Corresponding author: Daniel B. Nothaft, daniel.nothaft@colorado.edu

Corresponding author: Alexis S. Templeton, alexis.templeton@colorado.edu

Abstract

The potential for molecular hydrogen (H_2) generated via serpentinization to fuel subsurface microbial ecosystems independent from photosynthesis has prompted biogeochemical investigations of serpentinization-influenced fluids. However, investigations typically sample via surface seeps or open-borehole pumping, which can mix chemically distinct waters from different depths. Depth-indiscriminate sampling methods could thus hinder understanding of the spatial controls on nutrient availability for microbial life. To resolve distinct groundwaters in a low-temperature serpentinizing environment, we deployed packers (tools that seal against borehole walls during pumping) in two 400 m-deep, peridotite-hosted wells in the Samail Ophiolite, Oman. Isolation and pumping of discrete intervals as deep as 108 m to 132 m below ground level revealed multiple aquifers that ranged in pH from 8 to 11. Chemical analyses and 16S rRNA gene sequencing of deep, highly-reacted $Ca^{2+}-OH^-$ groundwaters bearing up to 4.05 μmol·L^{-1} H_2, 3.81 μmol·L^{-1} methane (CH_4) and 946 μmol·L^{-1} sulfate (SO_4^{2-}) revealed an ecosystem dominated by Bacteria affiliated with the class Thermodesulfovibrionia, a group of chemolithoheterotrophs supported by H_2 oxidation coupled to SO_4^{2-} reduction. In shallower, oxidized $Mg^{2+}-HCO_3^-$ groundwaters, aerobic and denitrifying heterotrophs were relatively more abundant. High $\delta^{13}C$ and δD of CH_4 (up to 23.9 ‰ VPDB and 45 ‰ VSMOW, respectively), indicated microbial CH_4 oxidation, particularly in $Ca^{2+} - OH^-$ waters with evidence of mixing with $Mg^{2+}-HCO_3^-$ waters. This study demonstrates the power of spatially resolving groundwaters to probe their distinct geochemical conditions and chemosynthetic communities. Such information will help improve predictions of where microbial activity in fractured rock ecosystems might occur, including beyond Earth.

Plain Language Summary

Peridotite rocks can react with water to form hydrogen gas. Microbes can combine hydrogen with oxidants to power their cells. Rocks similar to peridotite have been abundant throughout the history of Earth and the Solar System. Therefore, peridotite-water interaction is important for understanding the history and distribution of life. Prior studies investigating these processes have sampled waters from the surface of peridotite exposures or from open wells. These sampling methods risk contaminating deep, peridotite-hosted waters with shallower waters influenced by the atmosphere. In this study, we used packers (tools that can be used to pump waters from separate regions of the subsurface in isolation) to better understand the distribution of microbes and nutrients in subsurface peridotites. We sampled waters from separate subsurface zones as deep as 108 m to 132 m in two wells in peridotite. Waters from different depths had distinct chemical compositions and microbial communities. Sulfate reducing bacteria were dominant in waters that had most extensively reacted with peridotite in isolation, while microbes that consume nitrate or oxygen were also prevalent in waters with more evidence of atmospheric influence. The advanced sampling techniques we used help to distinguish where and how microbes live in the subsurface.

1 Introduction

Serpentinization reactions between peridotite and water can generate molecular hydrogen (H_2), and drive the reduction of carbon dioxide (CO_2) to organic acids such as formate ($HCOO^-$), and methane (CH_4) (Neal & Stanger, 1983; McCollom & Bach, 2009; McCollom & Seewald, 2003; Miller et al., 2017; Etiope et al., 2018; Klein et al., 2019), powerful electron donors that may fuel non-photosynthetic, subsurface microbial communities (Nealson et al., 2005). The potential relevance of such ecosystems to subsurface life on the modern and early Earth, as well as life beyond Earth, has led to numerous biogeochemical investigations of groundwaters from peridotite aquifers. These studies have primarily focused on groundwater samples from surface seeps or open-well pump-

ing (W. Brazelton et al., 2012; Chavagnac, Monnin, et al., 2013; Chavagnac, Ceuleneer, et al., 2013; Morrill et al., 2013; Suzuki et al., 2013, 2014; Crespo-Medina et al., 2014; Meyer-Dombard et al., 2015; Woycheese et al., 2015; Postec et al., 2015; Rempfert et al., 2017; Canovas III et al., 2017; W. J. Brazelton et al., 2017; Crespo-Medina et al., 2017; Suzuki et al., 2017; Marques et al., 2018; Nothaft et al., 2020; Leong et al., 2020). While these studies have transformed the understanding of the chemistry and biology of peridotite-hosted ecosystems, the sampling methods tend to yield mixtures of deep fluids with atmospherically influenced shallow fluids that were hydrologically segregated prior to sampling. This, in turn, can make it difficult to differentiate the sources, residence times, and geochemical states of fluids in serpentinizing systems, all of which influence the availability of nutrients to support endogenous microbial communities. For example, samples may be mixtures of surface-influenced groundwaters containing dissolved inorganic carbon ($\sum CO_2$), O_2, and nitrate (NO_3^-) and deeper groundwaters rich in H_2, CH_4, and sulfate (SO_4^{2-}). Downstream analyses of samples of potentially mixed origin therefore may obscure understanding of the subsurface peridotite-hosted biosphere.

The few hydrologic studies of ophiolite aquifers conducted to date show that groundwater flow is fracture-dominated, that fractures occur on multiple spatial scales, and that they are heterogeneously distributed, although generally more abundant within ~ 50 m to ~ 100 m of the surface (Boronina et al., 2003; Dewandel et al., 2005; Segadelli et al., 2017; Jeanpert et al., 2019; Lods et al., 2020). When deep, long-residence time groundwaters approach the surface, they have the potential to mix with lower-residence time groundwaters hosted in shallow, relatively high-transmissivity fracture networks (Paukert Vankeuren et al., 2019). This mixing may often be overlooked because groundwater pH is commonly used as an indicator of the extent of reaction of the water with peridotite out of contact with the atmosphere (with highly reacted waters being hyperalkaline, often defined as pH > 11), but pH is weakly sensitive to mixing of hyperalkaline groundwaters with circumneutral to moderately alkaline (pH 7 to 9) groundwaters derived from water-rock reaction in contact with the atmosphere (Leong et al., 2020).

In this study, we directly assessed the relationship between spatially heterogeneous hydrogeochemical parameters and subsurface microbial community compositions in ophiolite aquifers through the use of packers (tools that can be inflated at determined depths to seal against borehole walls during pumping). The use of packers allowed us to sample groundwaters from discrete, isolated depth intervals within two 400 m-deep wells in the Samail Ophiolite, Oman. We obtained depth-resolved aqueous geochemical data from both downhole wireline logging and measurements of solute concentrations in groundwater samples pumped from defined packer intervals. Gases (H_2, CO, and alkanes) dissolved in the pumped groundwaters were analyzed for their aqueous concentrations and their stable isotopic compositions (CH_4 and C_2H_6 only). Microbial community compositions of filter-concentrated biomass were assessed through 16S rRNA gene sequencing of extracted DNA. We accessed discrete aquifers at multiple depths, which ranged in pH from 8 to 11 and hosted distinct microbial communities. The deployment of packers to probe the biogeochemistry of subsurface, peridotite-hosted aquifers as presented herein marks a considerable advance in the ability to sample deep, serpentinization-influenced fluids isolated from surficial fluids and assess the effect of mixing these fluids on microbial processes. In doing so, this study furthers understanding of where and how serpentinization-influenced ecosystems may occur in the subsurface of Earth and celestial rocky bodies.

2 Site and methods

2.1 Site description and drilling

The Oman Drilling Project established a multi-borehole observatory (MBO) in Wadi Lawayni in the Wadi Tayin massif of the Samail Ophiolite (P. Kelemen et al., 2013, 2020). The initial hydrological characterization of the MBO has been previously described in

detail (Lods et al., 2020). Here, we focus on two 400 m deep, 6-inch diameter, rotary-drilled wells, BA1A and BA1D (Figure S1). Well BA1A was drilled in 2017, from February 20th to March 2nd, and BA1D was drilled in 2018, from February 24th to March 15th. These wells are situated in the mantle section of the ophiolite, 3 km north of the crust-mantle transition zone, and are spaced 15 m apart from one another. Shallow alluvium was isolated from the boreholes by installing casing during drilling. The casing extends to 21 m below ground level in BA1A and 26 m below ground level in BA1D (Figure 1). Below the surficial alluvium, drill cuttings from these wells were predominantly fully serpentinized dunite in the upper 160 m to 250 m and partially serpentinized harzburgite at greater depths (Figure 1; (P. Kelemen et al., 2020)). The drilling fluid was a mixture of 1 volume percent "DrillFoam," a biodegradable sodium alcohol ethoxyl sulfate with chelating agents, and 99 volume percent fresh water sourced from wells elsewhere in the region. BA1A and BA1D were air lift tested immediately after well completion for well development. The air lift tests involved pumping a mixture of water and air into the well at different depths and monitoring the air-lifted discharge.

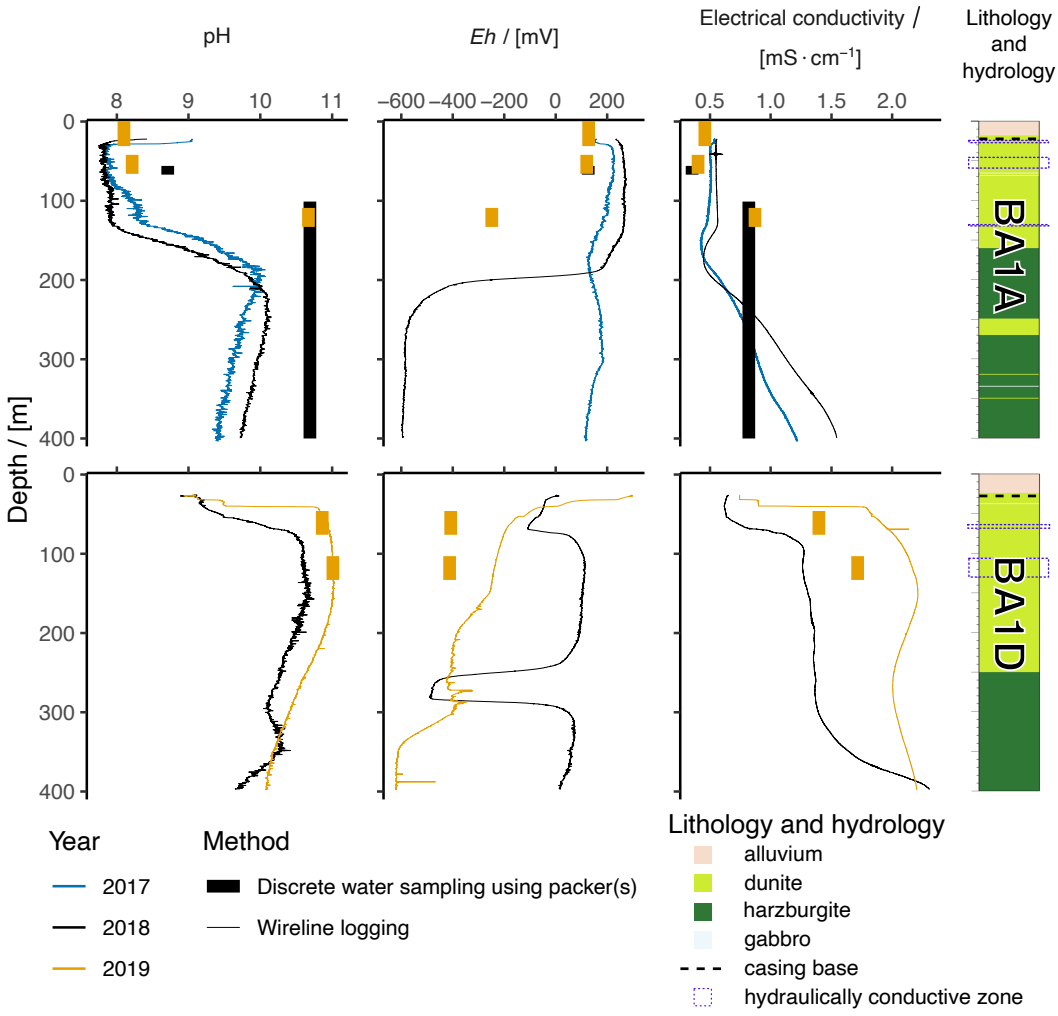

Figure 1. Biogeochemical trends with depth in BA1A and BA1D. *Eh*, pH, and electrical conductivity from well logs and pumped samples. All depths referenced to ground level. Well log data above casing base not shown. Well lithology from P. Kelemen et al. (2020). Hydraulically conductive zones sampled in this study had hydraulic conductivities of $10^{-6}\,\mathrm{m\,s^{-1}}$ to $10^{-2}\,\mathrm{m\,s^{-1}}$ (Lods et al., 2020).

2.2 Fluid sampling and field measurements

Downhole wireline logs (Matter et al., 2018) were obtained using an ALT QL40 OCEAN multi parameter probe, from which temperature, electrical conductivity, pH, and oxidation-reduction potential are reported with accuracy/precision of 0.005/0.001 °C, 5/0.1 μS · cm^{-1}, 0.01/0.001, and 1/0.1 mV, respectively. BA1A was logged on April 22$^{\mathrm{nd}}$, 2017 and March 16$^{\mathrm{th}}$, 2018. BA1D was logged on March 19$^{\mathrm{th}}$, 2018 and February 13$^{\mathrm{th}}$, 2019.

The packer system (Solexperts) includes two inflatable rubber bladders ("packers") and a submersible pump (Grundfos SQE 1–140) (Lods et al., 2020). Inflating one or both of the packers at depth in a well enables the isolation of discrete subsurface intervals for targeted pumping. The depth intervals from which samples were collected in this study are reported in Table 1. The sampling setup is pictured in Figure S2. At least the volume of water in subsurface pipes was pumped and discarded prior to taking samples of

groundwater. Temperature, pH, electrical conductivity, and oxidation-reduction potential (Eh), were monitored with probes at the pump outflow before and during sampling. The values of these parameters reported in Table 1 reflect the last measurements before the start of sampling for geochemical and microbiological analyses. Shorthand sample identifiers used throughout this manuscript consist of a well name, sampling year, and sampling interval, all concatenated (see Tables 1 and 2).

Table 1. Pumping data and field measurements.

Well	Sampling date			Sampling interval / [m]		Initial depth to water / [m]	Conductivity / $[\mathrm{mS \cdot cm^{-1}}]$	Temperature / [°C]	pH	Eh/ [mV]
	Year	Month	Day	Top	Bottom					
BA1A	2018	2	2	55	66	13.47	0.353	35.7	8.71	126
			8	100	400 (open)		0.820	37.5	10.69	n.d.
	2019	1	14	0 (open)	30	17.25	0.458	34.9	8.10	128
			16	41	65		0.402	35.0	8.21	120.
			16	108	132		0.871	36.5	10.67	−249
BA1D	2019	1	11	45	75	17.03	1.40	34.6	10.86	−408
			13	102	132		1.72	35.2	11.01	−412

Depths referenced to casing top. "n.d." = "not determined."

Table 2. Chemical composition of water samples.

Sample ID	$\sum \mathrm{CO_2}$	$\sum \mathrm{Na}$	$\sum \mathrm{Ca}$	$\sum \mathrm{Mg}$	$\sum \mathrm{Si}$	$\mathrm{NO_3^-}$	$\mathrm{SO_4^{2-}}$	$\mathrm{Cl^-}$
BA1A_2018_55-66	1.32×10^3	8.36×10^2	3.91×10^2	7.06×10^2	1.97×10^2	2.40×10^2	2.70×10^2	1.27×10^3
BA1A_2018_100-400	3.74×10^1	2.81×10^3	1.57×10^3	5.00×10^1	4.49×10^1	1.85×10^2	5.18×10^2	4.65×10^3
BA1A_2019_0-30	3.18×10^3	5.13×10^2	5.89×10^2	1.38×10^3	3.33×10^2	1.21×10^2	3.21×10^2	9.34×10^2
BA1A_2019_41-65	1.42×10^3	6.83×10^2	3.64×10^2	1.05×10^3	1.56×10^2	9.03×10^1	3.36×10^2	1.27×10^3
BA1A_2019_108-132	$< 2.82 \times 10^2$	3.36×10^3	1.69×10^3	1.02×10^1	2.13×10^1	$< 8.06 \times 10^{-1}$	4.67×10^2	5.96×10^3
BA1D_2019_45-75	n.d.	4.03×10^3	2.55×10^3	2.20×10^1	8.51	$< 8.06 \times 10^{-1}$	9.46×10^2	8.51×10^3
BA1D_2019_102-132	n.d.	5.18×10^3	2.92×10^3	1.56	5.88	$< 8.06 \times 10^{-1}$	5.91×10^2	6.87×10^3

Concentrations reported in $\mu\mathrm{mol \cdot L^{-1}}$. $\sum$ indicates the sum of all dissolved species of the element. "n.d." = "not determined."

2.3 Chemical and stable isotopic analyses of fluids

Chemical and stable isotopic analyses of fluids sampled in 2018 were conducted according to the methods reported by Nothaft et al. (2020). Analytical methods for fluids sampled in 2019 were similar and are reported below. To analyze aqueous concentrations (c) of non-carbonaceous chemical species, samples were collected by passing groundwater through a 0.2 μm filter into polypropylene conical tubes. Solutes that were readily positively ionizable were measured by inductively coupled plasma atomic emission spectroscopy (repeatability as median relative standard deviation of 3 % for most elements). Aqueous concentrations of $\mathrm{F^-}$ $\mathrm{Cl^-}$, $\mathrm{SO_4^{2-}}$, $\mathrm{Br^-}$, and $\mathrm{NO_3^-}$ were measured by ion chromatography (analytical uncertainty of 5 %). Molybdate-reactive $\mathrm{SiO_2}$ (reported here as $\sum \mathrm{Si}$) was quantitated using a spectrophotometric method (ASTM, 2016) (uncertainty of 2 % of measured value). The concentration and $\delta^{13}\mathrm{C}$ of dissolved inorganic C ($\sum \mathrm{CO_2}$) were measured by acidification of water samples and transfer of resultant $\mathrm{CO_2}$ (g) via a Thermo Fisher GasBench II to a Thermo Delta V Plus isotope ratio mass spectrometer. Details of $\sum \mathrm{CO_2}$ analyses are available at `http://dx.doi.org/10.17504/protocols.io.zduf26w`.

Groundwaters and gases dissolved therein were sampled via syringe from a luer-lok port on the pump manifold. 60. mL of this water was passed through a 0.2 μm filter and needle into an evacuated 117 mL glass vial capped with a blue chlorobutyl rubber stopper and Al crimp top. These are referred to as "headspace" samples. In addition, gases were sampled with the "bubble strip" method modified from Kampbell et al.

(1998). Details on bubble strip gas sampling are available at `http://dx.doi.org/10.17504/protocols.io.bkb9ksr6`. H_2, CH_4, and CO concentrations in this study are reported from headspace samples due to the better accuracy of this method versus the bubble strip method, as determined in comparisons by the authors. Ethane through hexane concentrations were determined from the bubble strip samples because of the lower detection limit offered by bubble strip samples, and were normalized to the headspace gas samples through the CH_4 concentration and assumption of constant C_1/C_n ratio of both sample types, where C_n is an alkane of n C atoms. Gas concentrations were determined according to the methods of Nothaft et al. (2020).

Bulk stable isotope analyses of CH_4 and co-occurring alkane gases were conducted at the University of Colorado - Boulder (CUB) by GC/C/Pyr/IRMS using a Trace 1310 GC equipped with an Agilent J & W GS-CarbonPLOT column (30 m length, 0.32 mm ID, 3.0 μm film) coupled to a Thermo Scientific MAT253 IRMS. Three CH_4 isotope standards purchased from Airgas (uncertainties of ± 0.3 ‰ for δ^{13}C and ± 5 ‰ for δD) and three additional standards obtained from the U.S. Geological Survey (uncertainties of ± 0.2 ‰ for δ^{13}C and ± 3 ‰ for δD) were used for calibration. Over the range of peak amplitudes of analyses reported here, the repeatability expressed as 1 s on analyses of standards is ± 0.2 ‰ for δ^{13}C and ± 3 ‰ for δD. The analytical uncertainty (accuracy) expressed as 1 standard error on a 3-point calibration was 0.4 ‰ to 0.7 ‰ for δ^{13}C and 4 ‰ to 5 ‰ for δD.

2.4 16S rRNA gene sequencing and analysis

Biomass for DNA extraction was concentrated by pumping 5 L to 20 L of groundwater through sterile Millipore polycarbonate inline filters. In 2018, groundwaters were passed sequentially through filters with pore diameters of 0.45 μm, 0.22 μm, then 0.10 μm to test whether cell size and microbial community composition were correlated. In 2019, only 0.22 μm pore diameter filters were used. The diameter of filters was 47 mm in both years. Filters were placed in cryovials and stored for transport in liquid N_2 dewars immediately following biomass collection. Upon their arrival at CUB, filters were stored in a -70 °C freezer until extraction.

For samples collected in 2018, DNA was extracted from one quarter subsamples of each filter using a Qiagen PowerSoil DNA extraction kit following manufacturer instructions, with the substitution of a 30-second bead beating step using a FastPrep-24 (MP Bio) homogenizer (instead of a standard vortexer) to more aggressively lyze cells. The V4 hypervariable region of the 16S rRNA gene was amplified by PCR in duplicate reactions using the 515 (Parada) - 806R (Apprill) primer pair modified to include Illumina adapters and the appropriate error-correcting barcodes, as described previously (Nothaft et al., 2020). Amplicons from duplicate reactions were pooled, cleaned, and their concentrations normalized using a Thermo Fisher SequalPrep normalization plate kit. Amplicons were sequenced on an Illumina MiSeq at the CUB Next-Generation Sequencing Facility using 2-by-150 bp paired-end chemistry.

For samples collected in 2019, DNA was extracted using the same methods as for 2018 samples. The V4 hypervariable region of the 16S SSU rRNA gene was amplified from purified DNA by PCR. PCR was performed in triplicate reactions using the 515 (Parada) - 806R (Apprill) primer pair at an annealing temperature of 50C, as described previously (Hamilton et al., 2013). Amplicons from triplicate reactions were pooled, and adapters were added in triplicate reactions via five cycles of nested PCR (following the same conditions as above) with 515 (Parada) - 806R (Apprill) primers modified to include Illumina adapters. Amplicons from triplicate reactions were pooled and purified using the Wizard PCR Preps DNA Purification System (Promega Corp.). Amplicons were sequenced on an Illumina Miseq at the UW-Madison Biotechnology Center DNA Sequencing Facility using 2-by-150 bp paired-end chemistry.

Demultiplexed fastq files were quality filtered using Figaro v1.1.1 (`https://github.com/Zymo-Research/figaro`) and the DADA2 v1.16 R package (Callahan et al., 2016). Amplicon sequence variants were assigned taxonomy to the genus level using the RDP classifier (Q. Wang et al., 2007) trained on the Silva SSU 138 reference database (Quast et al., 2012) using the DADA2 assignTaxonomy function. Sequences assigned to mitochondria, chloroplast, and Eukaryota, or not assigned at the domain level (collectively $< 1\,\%$ of sequences), were removed.

3 Prior study of site hydrology

To provide context for the geochemical results that will follow, we summarize here the findings of Lods et al. (2020), who interpreted flowmeter and pumping test data to understand the physical hydrology of boreholes BA1A and BA1D. The present study's samples from 2019 (Table 1) were collected simultaneously with, or immediately following, the pumping tests of Lods et al. (2020). Pumping depth intervals targeted hydraulically conductive zones in the subsurface, which were inferred from temperature profiles and flowmeter data (Lods et al., 2020). All hydraulically conductive regions were above the transition from dunite to harzburgite, which occurs at depths of 160 m in BA1A and 250 m in BA1D (Figure 1; (P. Kelemen et al., 2020)).

Flowmeter tests under ambient and forced hydraulic conditions indicated the presence of an aquifer in the highly weathered dunite bedrock at the contact between alluvium and bedrock immediately below the casing at 22 m to 25 m in BA1A and 26 m to 27 m in BA1D. The transmissivity in the shallow regions of BA1A was higher than in BA1D, and an ambient downflow of $1\,\mathrm{L{\cdot}min^{-1}}$ measured in BA1A from 22 m to 59 m indicated the displacement of substantial volumes of water from the surficial highly weathered dunites aquifer to lower dunite aquifers at BA1A at least as deep as 59 m. Lesser flow may extend to even deeper aquifers at BA1A at rates below the detection limit of the flowmeter used in the experiments of Lods et al. (2020) ($< 0.1\,\mathrm{L \cdot min^{-1}}$). Ambient flow was below detectable levels at BA1D, suggesting minimal flow of surficial aquifer waters to deeper aquifers at BA1D.

In conductive fractures between 41 m and 75 m depth, tests of pumping in BA1A indicated channelized, 1-dimensional flow between BA1A and BA1D. This flow was interpreted as passing through an open or partially mineralized fracture connected to the boreholes directly or through a conduit. All the pumped flow from BA1A in that interval could be accommodated through this channel. However, during pumping of BA1D in that interval, additional vertical flow from the formation near BA1D above and below the pumped interval was required to accommodate the pumped flow.

In contrast to the 41 m to 75 m aquifer, an aquifer between 102 m and 132 m displayed no evidence of conductive structures with channelized flow. Rather, heterogeneities in the directions of flow contributing to the pumping tests were inferred. The pumping in BA1A was supplied by both horizontal and vertical flows that were both near and far from the pumped borehole. Pumping in BA1D was also supplied by horizontal and vertical flows near the pumped borehole, but only horizontal flows further away, near BA1A. Lods et al. (2020) speculated that a component of the water pumped during the BA1D test could have been derived from the highly conductive fractures in the shallower regions near BA1A, with this water flowing downward through the BA1A borehole and then horizontally to BA1D via fractures in the 102 m and 132 m depth interval.

Below 133 m, BA1D had sufficient transmissivity to accomodate pumping, but samples were not obtained from this interval for the present study due to low sustainable flow rates ($0.5\,\mathrm{L{\cdot}min^{-1}}$). Vertical connections around BA1D link depths below 133 m to the 102 m and 132 m conductive interval of BA1D (and then to BA1A via horizon-

tal connections). Vertical connections surrounding BA1A below 133 m were comparatively weaker, preventing successful pumping from this region of BA1A.

4 Results

4.1 Aquifer geochemistry: drilling, mixing, and recovery

During drilling, a strong smell of sulfide was evident within tens of meters of BA1A, suggesting sulfidic conditions in the subsurface at the time of drilling. In well logs acquired shortly after drilling of BA1A in 2017 and BA1D in 2018, *Eh* values were 100 mV to 200 mV throughout most of the depth profile (Figure 1), indicating the presence of oxidized fluids that were likely introduced at depth through drilling. In well logs obtained at BA1A in 2018, a year after the drilling of that well, the chemical state of the upper 200 m of the depth profile was essentially unchanged since 2017, but the lower 200 m of the depth profile showed a pH increase of 0.4 (reaching a maximum pH of 10.15), a stark *Eh* decrease of 800 mV (reaching a minimum of −599 mV), and an electrical conductivity increase of up to 0.3 mS·cm^{-1} (reaching a maximum of 1.544 mS·cm^{-1}). These data indicate at least partial recovery towards reduced, hyperalkaline conditions at depths > 200 m at BA1A from 2017 to 2018. Similarly, in BA1D well logs obtained in 2019, a year after the drilling of that well, a pH increase of 0.5 (reaching a maximum of pH of 11.05), a stark *Eh* decrease of up to 700 mV (reaching a minimum of −623 mV), and an electrical conductivity increase of up to 0.8 mS·cm^{-1} (reaching 2.21 mS·cm^{-1}) relative to the 2018 log were observed throughout most of the depth profile. A notable difference between BA1A and BA1D well logs recorded a year after drilling is that the conditions in BA1A transition from moderately alkaline and oxidized to hyperalkaline and reduced at $\sim$ 150 m depth, while in BA1D, hyperalkaline and reduced conditions are reached at relatively shallow depths (40 m) and maintained to the bottom of the well (Figure 1).

The *Eh*, pH, and electrical conductivity in about half of the samples pumped from discrete intervals using packers are similar to values at the same depth in the well logs obtained a year after drilling. The other half of the samples have *Eh*, pH, and/or conductivity that are different from well log values at the same depth. For instance, the packer samples BA1A_2018_100-400 and BA1A_2019_108-132 had higher pH values than in the downhole log at any depth, and show pH > 10 at a much shallower depth than in the 2018 log, where such high pH is only reached below 200 m. At BA1D, pH values of pumped samples from 2019 overlap with those of well logs measured in the same year and at equivalent intervals, but the pumped samples had *Eh* values 200 mV lower and electrical conductivity values 0.5 mS $\cdot$ cm^{-1} lower than the well logs at the same depths.

As expected based on pH, *Eh*, and electrical conductivity (Figure 1, Table 1), the pH 8.1 to 8.7 waters in the upper 70 m of BA1A are $Mg^{2+}-HCO_3^-$ waters. The pH 10.6 to 11.0 waters at both sampled depths in BA1D and in the $\geq$ 100 m-depth samples from BA1A are $Ca^{2+} - OH^-$ waters (Table 2). These are the two commonly observed water end-members in ophiolite aquifers, where $Mg^{2+} - HCO_3^-$ waters are considered to communicate openly with the atmosphere and have shorter residence times, while $Ca^{2+}-OH^-$ waters have extensively reacted with peridotite in regions of the subsurface closed to atmospheric inputs (Barnes et al., 1967; Barnes & O'Neil, 1969; Neal & Stanger, 1985; Bruni et al., 2002; Cipolli et al., 2004; P. B. Kelemen & Matter, 2008; P. B. Kelemen et al., 2011; A. N. Paukert et al., 2012; Chavagnac, Monnin, et al., 2013; Boulart et al., 2013; Canovas III et al., 2017; Leong & Shock, 2020). These water types have distinct $\sum$Si concentrations, as mineral dissolution in waters open to the atmosphere increases $\sum$Si in $Mg^{2+} - HCO_3^-$ waters to 10^2 μmol $\cdot$ L^{-1} concentrations, while reaction under closed system, lower water/rock conditions in $Ca^{2+}-OH^-$ waters approaches chrysotile-brucite-calcite-diopside equilibrium and draws $\sum$Si to μmol·L^{-1} to 10^2 nmol·L^{-1} concentrations (Leong et al., 2020). Leong et al. (2020) proposed the use of $\sum$Si as a tracer of mixing in ophiolitic groundwaters, noting its relatively conservative behavior in these

systems and its stronger sensitivity to mixing relative to pH. Adopting this approach, we have plotted the $c_{\sum \mathrm{Si}}$ and pH of our samples in Figure 2. The shallowest sample in this study, BA1A_2019_0-30, had the highest $c_{\sum \mathrm{Si}}$ of the data set ($333\,\mu\mathrm{mol{\cdot}L^{-1}}$), which is typical of $\mathrm{Mg^{2+}}-\mathrm{HCO_3^-}$ waters. Other samples fall below this, but do not reach the low levels representative of chrysotile-brucite-calcitediopside equilibrium as in end-member $\mathrm{Ca^{2+}}-\mathrm{OH^-}$ waters, suggesting that they represent mixtures of varying proportions of $\mathrm{Mg^{2+}}-\mathrm{HCO_3^-}$ and $\mathrm{Ca^{2+}}-\mathrm{OH^-}$ end-member waters.

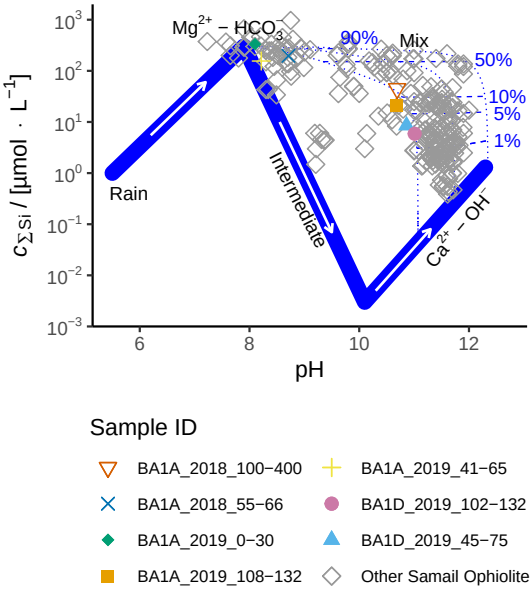

Figure 2. $\sum$Si vs. pH plot, after Leong et al. (2020). The thick blue line corresponds to the reaction path model of Leong et al. (2020) starting from rain, progressing to moderately alkaline $\mathrm{Mg^{2+}}-\mathrm{HCO_3}$ waters as a response to mineral dissolution open to the atmosphere, then intermediate waters in early stages of serpentinization closed to the atmosphere, which later become hyperalkaline $\mathrm{Ca^{2+}}-\mathrm{OH^-}$ waters as they approach chrysotile-brucite-calcitediopside equilibrium. Three potential end member $\mathrm{Ca^{2+}}-\mathrm{OH^-}$ water compositions (differing in their $c_{\sum \mathrm{CO_2}}$ from $8\,\mu\mathrm{mol\cdot kg^{-1}}$ to $20\,\mu\mathrm{mol\cdot kg^{-1}}$) form one side of a mixing trend to a typical $\mathrm{Mg^{2+}}-\mathrm{HCO_3}$ water composition. Si, which is the most conservative tracer of mixing available in ophiolites, is used to distinguish extents of mixing between $\mathrm{Ca^{2+}}-\mathrm{OH^-}$ and $\mathrm{Mg^{2+}}-\mathrm{HCO_3}$ waters (shown in plot as percentages next to mixing tie-lines). Mixing extents calculated for our samples are tabulated in Table S1. Other Samail Ophiolite data from (Neal & Stanger, 1985; Chavagnac, Monnin, et al., 2013; Miller et al., 2016; Rempfert et al., 2017; Canovas III et al., 2017; ?, ?; Nothaft et al., 2020; Paukert Vankeuren et al., 2019; Leong et al., 2020)

In the $\mathrm{Mg^{2+}}-\mathrm{HCO_3^-}$ waters in the upper 70 m of BA1A, dissolved inorganic carbon ($\sum \mathrm{CO_2}$) ranged in concentration (c) from $1320\,\mu\mathrm{mol{\cdot}L^{-1}}$ to $3180\,\mu\mathrm{mol{\cdot}L^{-1}}$, similar to $c_{\sum \mathrm{CO_2}}$ in other $\mathrm{Mg^{2+}}-\mathrm{HCO_3^-}$ waters in the ophiolite (Neal & Stanger, 1985; Chavagnac, Monnin, et al., 2013; Rempfert et al., 2017; Canovas III et al., 2017; Paukert Vankeuren et al., 2019; Nothaft et al., 2020; Leong et al., 2020), and consistent with uptake of atmospheric $\mathrm{CO_2}$ into these moderately alkaline waters (Bruni et al., 2002; Cipolli et al., 2004; A. N. Paukert et al., 2012; Leong & Shock, 2020). In the $\mathrm{Ca^{2+}}-\mathrm{OH^-}$ waters sampled at ≥ 100 m depths at BA1A, $c_{\sum \mathrm{CO_2}}$ was $37.4\,\mu\mathrm{mol{\cdot}L^{-1}}$ in 2018 and be-

low the limit of quantitation in 2019 ($< 282\,\mu mol{\cdot}L^{-1}$; Table 2). Hyperalkaline groundwaters sampled from certain other wells in 2018, including the nearby (within 2 km), pH $\sim$ 11.4 well, NSHQ14, for which $c_{\sum CO_2}$ was measured in the same analytical session as BA1A_2018_100-400, had $c_{\sum CO_2}$ below the limit of quantitation in 2018 ($< 12\,\mu mol{\cdot}L^{-1}$; (Nothaft et al., 2020)).[1] These lower values are consistent with water-harzburgite reaction path modeling that terminates at chrysotile-brucite-diopside-calcite equilibrium, corresponding to a $c_{\sum CO_2}$ of $8\,\mu mol \cdot L^{-1}$ at 25 °C and 1 bar (Leong & Shock, 2020). Thus, the relatively higher $c_{\sum CO_2}$ in BA1A_2018_100-400 suggests that this sample does not represent $Ca^{2+}-OH^-$ end-member water, but rather is the product of groundwater mixing or moderate extents of water-rock reaction. Though not on the compositional extremes of peridotite-hosted groundwaters, $\sum CO_2$ concentrations in the tens of $\mu mol{\cdot}L^{-1}$ or less in the $Ca^{2+}-OH^-$ waters of BA1A and BA1D are still quite low compared to seawater at $2.1\,mmol \cdot L^{-1}$ or river water at $50\,\mu mol \cdot L^{-1}$ to $500\,\mu mol \cdot L^{-1}$ (Zeebe & Wolf-Gladrow, 2001; Waldron et al., 2007).

Concentrations of the reduced gases H_2 and CH_4 ranged up to $4.05\,\mu mol{\cdot}L^{-1}$ and $3.81\,\mu mol \cdot L^{-1}$, respectively, in $Ca^{2+} - OH^-$ waters of BA1A and BA1D, whereas H_2 and CH_4 were below limits of quantitation in the $Mg^{2+} - HCO_3^-$ waters from the upper 70 m of BA1A (Table 3), consistent with the differing Eh of these waters (Table 1). The concentrations of H_2 and CH_4 in the $Ca^{2+} - OH^-$ waters are high in comparison to near-surface aquifers in sedimentary settings, where H_2 concentrations rarely exceed $10\,nmol \cdot L^{-1}$, even under the most reduced conditions (Lovley et al., 1994; Kampbell et al., 1998), but they are moderate in the context of peridotite aquifers, as in the Samail Ophiolite, where groundwaters accessed at wells can have H_2 and CH_4 concentrations in the hundreds to thousands of $\mu mol{\cdot}L^{-1}$ (A. Paukert, 2014; Nothaft et al., 2020). In addition, dissolved $C_2 - C_6$ alkanes were detected in some samples (Table 3). In samples with quantitatable C_2H_6, CH_4/C_2H_6 ratios ranged from 14.6 to 106, lower than $CH_4/(C_2H_6 \pm C_3H_8)$ ratios of 10^2 to 10^4 previously reported in other samples from the Samail Ophiolite (Figure S3; (Etiope et al., 2015; Vacquand et al., 2018; Nothaft et al., 2020)).

To assess the availability of oxyanions as terminal electron acceptors for microbial metabolism, NO_3^- and SO_4^{2-} concentrations were measured (Table 2). In samples of BA1A taken in 2018, NO_3^- concentrations were higher in samples from depths of 55 m to 66 m ($240.\,\mu mol \cdot L^{-1}$) than in samples from depths of 100 m to 400 m ($185\,\mu mol \cdot L^{-1}$). In samples of BA1A taken in 2019, a trend of decreasing $c_{NO_3^-}$ with increasing depth was also observed, with samples from depths of 0 m to 30 m, 41 m to 65 m, and 108 m to 132 m having NO_3^- concentrations of $132\,\mu mol \cdot L^{-1}$, $90.3\,\mu mol \cdot L^{-1}$, and below the limit of quantitation ($< 0.806\,\mu mol{\cdot}L^{-1}$), respectively. The higher NO_3^- concentrations are within the range previously reported for $Mg^{2+}-HCO_3^-$ waters sampled from wells in the ophiolite (Rempfert et al., 2017; Nothaft et al., 2020). NO_3^- was below the limit of quantitation in all samples from BA1D. Thus, concentrations of NO_3^- were higher in more oxidized aquifers at BA1A and BA1D (Table 1; Figure 1).

In contrast, SO_4^{2-} concentrations were generally higher in more reduced and hyperalkaline water samples (Table 2; Figure S5), reaching $946\,\mu mol{\cdot}L^{-1}$ in BA1D_2019_45-75. The higher SO_4^{2-} concentrations in BA1A and BA1D are higher than in other $Ca^{2+}-OH^-$ waters in the Samail Ophiolite, in which SO_4^{2-} concentrations are usually in the tens of $\mu mol \cdot L^{-1}$ and rarely exceed $500\,\mu mol \cdot L^{-1}$ (Figure S5). Compared to $Ca^{2+}-OH^-$ waters, SO_4^{2-} concentrations are typically higher in $Mg^{2+}-HCO_3^-$ waters ($100\,\mu mol{\cdot}$

[1] The limit of quantiation for $c_{\sum CO_2}$ was higher in 2019 than in 2018 because a set of higher volume samples from 2019 were compromised during transport. We usually take two different sample volumes to ensure that, upon acidification, both $Mg^{2+} - HCO_3^-$ and $Ca^{2+} - OH^-$ end-member waters have optimal m/z 44 signal intensity for mass spectrometer analysis.

[!h]

Table 3. Aqueous gas concentrations, reported in $\mu\text{mol} \cdot \text{L}^{-1}$.

Sample ID	H_2	CO	CH_4	C_2H_6	C_3H_8	i-C_4H_{10}	n-C_4H_{10}	i-C_5H_{12}	n-C_5H_{12}	C_6H_{14}[a]
BA1A_2018_55-66	$< 5.98 \times 10^{-1}$	$< 1.32 \times 10^{-1}$	$< 1.18 \times 10^{-1}$	$< 9.88 \times 10^{-4}$	$< 7.60 \times 10^{-4}$	$< 4.61 \times 10^{-4}$	$< 5.78 \times 10^{-4}$	$< 3.43 \times 10^{-4}$	$< 3.81 \times 10^{-4}$	$< 2.81 \times 10^{-4}$
BA1A_2018_100-400	4.05	$< 1.32 \times 10^{-1}$	2.42×10^{-1}	$< 9.88 \times 10^{-4}$	$< 7.60 \times 10^{-4}$	$< 4.61 \times 10^{-4}$	3.89×10^{-2}	$< 3.43 \times 10^{-4}$	$< 3.81 \times 10^{-4}$	8.80×10^{-4}
BA1A_2019_0-30	< 3.29	$< 2.04 \times 10^{-2}$	$< 6.70 \times 10^{-1}$	$< 8.63 \times 10^{-3}$	$< 6.81 \times 10^{-3}$	$< 4.13 \times 10^{-3}$	$< 5.45 \times 10^{-3}$	$< 3.27 \times 10^{-3}$	$< 3.63 \times 10^{-3}$	$< 2.77 \times 10^{-3}$
BA1A_2019_41-65	< 3.29	$< 2.04 \times 10^{-2}$	$< 6.70 \times 10^{-1}$	$< 8.63 \times 10^{-3}$	$< 6.81 \times 10^{-3}$	$< 4.13 \times 10^{-3}$	$< 5.45 \times 10^{-3}$	$< 3.27 \times 10^{-3}$	$< 3.63 \times 10^{-3}$	$< 2.77 \times 10^{-3}$
BA1A_2019_108-132	< 3.29	$< 2.04 \times 10^{-2}$	1.05	7.16×10^{-2}	$< 6.81 \times 10^{-3}$	$< 4.13 \times 10^{-3}$	$< 5.45 \times 10^{-3}$	$< 3.27 \times 10^{-3}$	$< 3.63 \times 10^{-3}$	$< 2.77 \times 10^{-3}$
BA1D_2019_45-75	< 3.29	$< 2.04 \times 10^{-2}$	2.30	2.16×10^{-2}	$< 6.81 \times 10^{-3}$	$< 4.13 \times 10^{-3}$	$< 5.45 \times 10^{-3}$	$< 3.27 \times 10^{-3}$	$< 3.63 \times 10^{-3}$	$< 2.77 \times 10^{-3}$
BA1D_2019_102-132	3.55	$< 2.04 \times 10^{-2}$	3.81	1.27×10^{-1}	$< 6.81 \times 10^{-3}$	$< 4.13 \times 10^{-3}$	$< 5.45 \times 10^{-3}$	$< 3.27 \times 10^{-3}$	$< 3.63 \times 10^{-3}$	$< 2.77 \times 10^{-3}$

[a]Hexane isomers not chromatographically resolved.

L^{-1} to $1000\,\mu mol \cdot L^{-1}$) and gabbro waters ($500\,\mu mol \cdot L^{-1}$ to $4000\,\mu mol \cdot L^{-1}$) in the Ophiolite (Figure S5). The co-existence of SO_4^{2-} approaching mmol·L^{-1} levels and H_2 at $\mu mol \cdot L^{-1}$ levels in some $Ca^{2+} - OH^-$ waters at BA1A and BA1D could make microbial SO_4^{2-} reduction coupled to H_2 oxidation a viable metabolic strategy in those waters.

4.2 Stable isotopic compositions of water, $\sum CO_2$, CH_4 and C_2H_6

To trace H and C through the BA1 system, the stable isotopic compositions of water, $\sum CO_2$, CH_4, and C_2H_6 were measured. Groundwater δD and $\delta^{18}O$ data plot near local and global meteoric water lines (Weyhenmeyer et al., 2002; Terzer et al., 2013), indicating that the groundwaters are derived from rain (Table 4; Figure S4; (Matter et al., 2006; Miller et al., 2016; Paukert Vankeuren et al., 2019; Nothaft et al., 2020)). The $\delta^{13}C_{\sum CO_2}$ of $Mg^{2+} - HCO_3^-$ waters in the upper 70 m of BA1A ranged from −14.64 ‰ VPDB to −14.15 ‰ VPDB (Table 4), which is within the range of $\delta^{13}C_{\sum CO_2}$ of $Mg^{2+} - HCO_3^-$ waters elsewhere in the ophiolite (−15.56 ‰ VPDB to −10.88 ‰ VPDB; (Matter et al., 2006; Nothaft et al., 2020)). These values are considerably lower than seawater $\delta^{13}C_{\sum CO_2}$, which ranges from 0 ‰ VPDB to 2 ‰ VPDB (Zeebe & Wolf-Gladrow, 2001). This difference is peculiar because, like seawater, $Mg^{2+} - HCO_3^-$ waters in ophiolites have HCO_3^- as the dominant $\sum CO_2$ species and are widely thought to be close to equilibrium with atmospheric CO_2 (Neal & Stanger, 1985; Bruni et al., 2002; Cipolli et al., 2004; A. N. Paukert et al., 2012; Leong & Shock, 2020). In comparison to the $Mg^{2+} - HCO_3^-$ water at BA1A, a deeper sample (BA1A_2018_100-400) bearing $Ca^{2+} - OH^-$ water had notably lower $\delta^{13}C_{\sum CO_2}$ (−18.0 ‰ VPDB; Table 4). The dynamics of $\delta^{13}C_{\sum CO_2}$ in this system will be discussed further in Section 5.4.

Table 4. Stable isotopic compositions of water, $\sum CO_2$, CH_4 and C_2H_6.

Sample ID	δD_{H_2O}	$\delta^{18}O_{H_2O}$	$\delta^{13}C_{\sum CO_2}$	$\delta^{13}C_{CH_4}$	δD_{CH_4}	$\delta^{13}C_{C_2H_6}$
BA1A_2018_55-66	−10.9	−2.55	−14.64	n.d.	n.d.	n.d.
BA1A_2018_100-400	−9.4	−2.17	−18.0	n.d.	n.d.	n.d.
BA1A_2019_0-30	−10.8	−2.44	−14.15	n.d.	n.d.	n.d.
BA1A_2019_41-65	−9.77	−2.27	−14.32	n.d.	n.d.	n.d.
BA1A_2019_108-132	−3.92	−0.91	n.d.	23.9	45	n.d.
BA1D_2019_45-75	−4.52	−1.04	n.d.	12.8	−111	n.d.
BA1D_2019_102-132	−6.9	−1.59	n.d.	3.8	−112	−2.5

All δ values reported in ‰ units. $\delta^{18}O$ and δD reported relative to VSMOW. $\delta^{13}C$ reported relative to VPDB. "n.d." = "not determined."

Three samples had sufficient CH_4 for accurate isotopic analysis using our methods (Table 4). BA1D_2019_102-132 had a $\delta^{13}C_{CH_4}$ of 3.8 ‰ VPDB, which is high compared to CH_4 typically found in sedimentary settings, but within the range of CH_4 in serpentinizing settings, including the Samail Ophiolite (Figure 3; (Milkov & Etiope, 2018)). BA1D_2019_45-75 had a $\delta^{13}C_{CH_4}$ of 12.8 ‰ VPDB, which is higher than previously reported for CH_4 in Samail Ophiolite, and BA1A_2019_108-132 had even higher $\delta^{13}C_{CH_4}$ (23.9 ‰ VPDB).

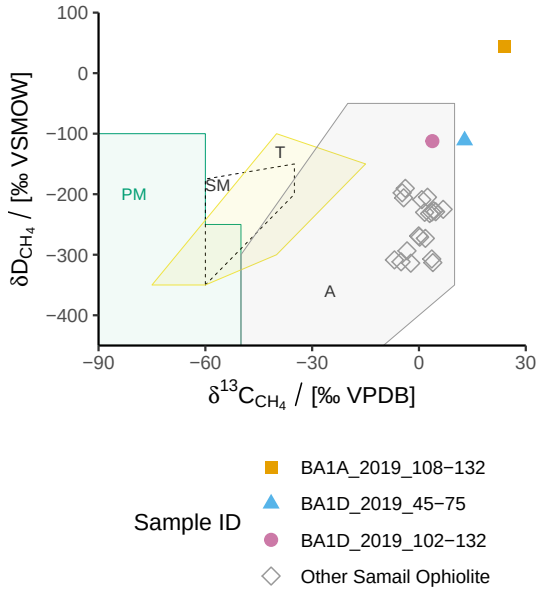

Figure 3. Plot of δD_{CH_4} vs. $\delta^{13}C_{CH_4}$ of samples from BA1A and BA1D with previously published Samail Ophiolite samples (Etiope et al., 2015; Vacquand et al., 2018; Nothaft et al., 2020) shown in black for context. Shaded fields of typical gas origin after Milkov and Etiope (2018). *Abbreviations:* PM, primary microbial; SM, secondary microbial; T, thermogenic; A, abiotic.

In addition to CH_4, there was sufficient C_2H_6 for isotopic analysis in sample BA1D_2019_102-132, and this C_2H_6 was also ^{13}C-enriched (−2.5 ‰ VPDB; Table 4) compared to C_2H_6 typically found in sedimentary settings (Prinzhofer & Huc, 1995). However, this $\delta^{13}C_{C_2H_6}$ value is generally similar to that previously reported for C_2H_6 in the Samail Ophiolite (Figure 4; (Fritz et al., 1992; Nothaft et al., 2020)), suggesting an abiotic source of C_2H_6 at BA1D. The $\delta^{13}C_{C_2H_6}$ of BA1D_2019_102-132 is notably similar (within 3.5 ‰) to $\delta^{13}C_{C_2H_6}$ of well NSHQ14 (Nothaft et al., 2020), which is only 2 km down-gradient within the same catchment, suggesting a similar source of C_2H_6 in these wells.

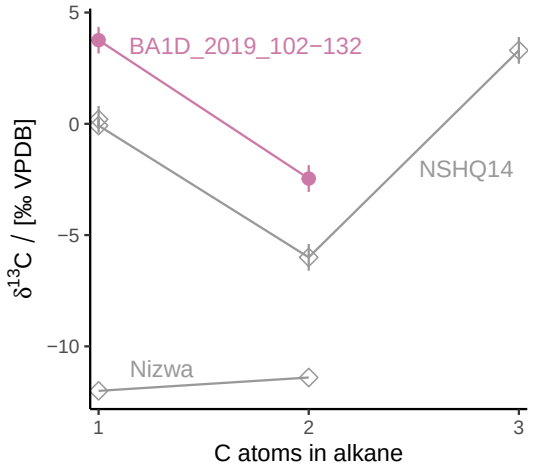

Figure 4. Plot of $\delta^{13}C$ of CH_4 and co-occurring n-alkanes vs. the number of C atoms per molecule. Error bars represent uncertainties on $\delta^{13}C$ analyses performed at CUB. Only samples for which $\delta^{13}C_{C_2}$ was determined are plotted. Contextual data from the Samail Ophiolite at Nizwa (Fritz et al., 1992) and well NSHQ14 (Nothaft et al., 2020).

The δD_{CH_4} at BA1D (−111 ‰ VSMOW to −112 ‰ VSMOW; Table 4) is higher than that of samples previously reported from the Samail Ophiolite (Figure 3), but similar to that of samples from sediment-poor seafloor hydrothermal vents that are near isotopic equilibrium with ocean water at 270 °C to 360 °C (D. T. Wang et al., 2018; Labidi et al., 2020) and similar to some samples from ophiolites, including those in the Philippines (Abrajano et al., 1990) and Turkey (Young et al., 2017), where dominantly abiotic sources of CH_4 have been proposed. Thus, it is plausible, from the perspective of δD_{CH_4}, that BA1D CH_4 formed abiotically and equilibrated, potentially at 270 °C to 360 °C, with water with δD similar to that of seawater. The δD_{CH_4} of BA1A_2019_108-132, however, is extraordinarily high (45 ‰ VSMOW). Noting that the δD of water at BA1A, BA1D, and other wells in the Samail Ophiolite is within 15 ‰ of VSMOW (Table 2; (Miller et al., 2016; Paukert Vankeuren et al., 2019; Nothaft et al., 2020)), the high δD of CH_4 from BA1A_2019_108-132 cannot plausibly be explained by CH_4 having equilibrated with water (Horibe & Craig, 1995). Moreover, it is unlikely to have been produced through kinetic processes, in which CH_4 would be expected to be D-depleted with respect to the H of its precursor. Thus, the δD_{CH_4} of BA1A_2019_108-132 likely indicates post-genetic fractionation, perhaps during microbial CH_4 oxidation. CH_4 oxidation is also compatible with the low $CH_4/(C_2H_6 + C_3H_8)$ in BA1A and BA1D samples, particularly BA1A_2019_108-132 ($CH_4/C_2H_6 = 14.6$), relative to other samples from the Samail Ophiolite (Figure S3).

4.3 16S rRNA gene sequencing

To assess microbial community composition, 16S rRNA genes of DNA extracted from biomass that was concentrated from groundwaters were amplified and sequenced. 16S rRNA gene reads affiliated with class Thermodesulfovibrionia were dominant in the BA1A and BA1D data set, accounting for more than 90 % of reads in some samples (Figure 5), particularly those with low *Eh* (Table 1). Cultured representatives of Thermodesulfovibrionia are capable of SO_4^{2-} reduction coupled to H_2 oxidation and may additionally/alternatively oxidize C_1-C_3 acids and use thiosulfate, sulfite, Fe^{3+} or NO_3^- as terminal electron acceptors for anaerobic respiration (Henry et al., 1994; Sekiguchi et al., 2008; Frank et al., 2016). The high relative abundance of Thermodesulfovibrionia, es-

pecially in samples that are reduced, contain up to μmol $\cdot$ L^{-1} levels of H_2, approach mmol$\cdot L^{-1}$ levels of SO_4^{2-}, and have below quantitatable (sub-μmol$\cdot L^{-1}$) levels of NO_3^-, suggests that microbial sulfate reduction may be an important process in the subsurface at BA1A and BA1D.

Taxa that had markedly higher relative abundances of 16S rRNA genes in the more oxidized waters sampled from the upper 70 m of BA1A include relatives of the genus *Brachymonas* and the species *Parvibaculum lavamentivorans* (Figure 5). Cultured representatives of *Brachymonas* are heterotrophic and respire using molecular oxygen, and in some cases nitrate, as terminal electron acceptors (Hiraishi et al., 1995; Halpern et al., 2009). A close relative of *Brachymonas denitrificans* was enriched with H_2 and formate using groundwater sampled from wells in the Coast Range Ophiolite, USA as innoculum (Crespo-Medina et al., 2014). This indicates that *Brachymonas* relatives can thrive in anaerobic conditions in serpentinization-derived fluids. *Parvibaculum lavamentivorans* isolates are aerobic heterotrophs (Schleheck et al., 2011), but *Parvibaculum* species have also been detected through culture-independent methods in enrichment cultures under anaerobic, denitrifying conditions (Blöthe & Roden, 2009; De Weert et al., 2011). The high relative abundances of *Brachymonas*- and *P. lavamentivorans*-affiliated 16S rRNA gene reads in the more oxidized parts of BA1A, taken together with the trends of decreasing $c_{NO_3^-}$ with increasing depth at BA1A (Section 4.1), suggest that heterotrophic, aerobic and/or denitrifying microbial metabolisms may be active in those regions of the subsurface.

Taxa that also had high 16S rRNA gene relative abundances in some samples, but whose metabolic functions are more enigmatic, include relatives of the genus *Meiothermus*. 16S rRNA gene reads affiliated with *Meiothermus* were detected in all BA1A and BA1D samples, but had the highest relative abundance (22 % of reads) in the sample BA1A_2018_100-400 (Figure 5). Although *Eh* was not directly measured for BA1A_2018_100-400, this sample had 4.05 μmol$\cdot L^{-1}$ H_2 (Table 3) and a pH of 10.69 (Table 2), suggesting that it was reduced, which would be consistent with a sample from a similar depth interval taken the following year (BA1A_2019_108-132), which had an *Eh* of −249 mV (Table 1). *Meiothermus* has been a confounding taxon in 16S rRNA gene surveys of the Samail Ophiolite subsurface because *Meiothermus* isolates reported in the literature have thus far been shown to be aerobic (although some can reduce NO_3^- to NO_2^-; (Habib et al., 2017; Raposo et al., 2019)). Nonetheless, *Meiothermus*-affiliated 16S rRNA gene sequences have consistently accounted for high percentages of reads from the most reduced (lowest f_{O_2}) groundwater samples from wells in the Samail Ophiolite, where they apparently cohabitate with obligate anaerobes (Miller et al., 2016; Rempfert et al., 2017; Nothaft et al., 2020; Kraus et al., 2021). Previous studies of the ophiolite have suggested that *Meiothermus* could have been functioning anaerobically, or could have been inhabiting shallow, oxic waters that were mixed with deeper, anoxic waters during open-borehole pumping (Miller et al., 2016; Rempfert et al., 2017). The present study's finding of high relative abundances of *Meiothermus* 16S rRNA gene reads in a sample obtained through pumping of a $>$ 100 m depth interval isolated using packers favors the interpetation that *Meiothermus* are indeed capable of functioning anaerobically in the subsurface. Cultivation approaches or metagenomic inferences of the functionality of these organisms based on gene complements will be required to determine how *Meiothermus sp.* persists in these highly reduced waters.

Another enigmatic taxon is candidate phylum GAL15, which comprised 26 % of 16S rRNA gene reads in the sample BA1D_2019_102-132 (Figure 5). No genomes or cultured isolates from this taxon have been published, so its traits can only be inferred indirectly. The relative abundance of GAL15 in 16S rRNA gene amplicon sequences and shotgun metagenomic sequences was found to positively correlate with increasing depth in a study of 20 soil profiles in diverse ecological settings throughout the United States, suggesting that members of GAL15 are well-suited to the oligotrophic conditions of relatively deep (1 m) soil horizons (Brewer et al., 2019). Members of GAL15 have also been

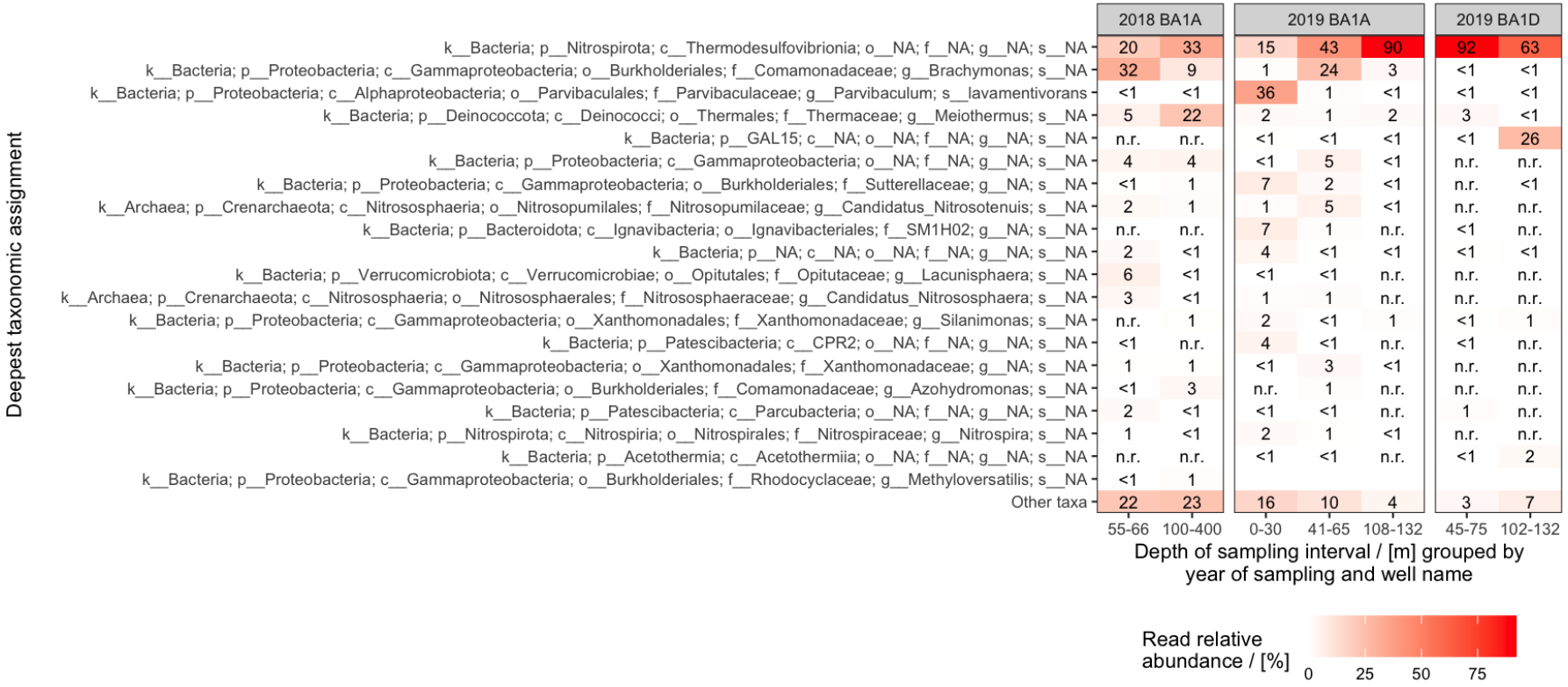

Figure 5. 16S rRNA gene read relative abundances of 20 most abundant taxonomic assignments in DNA extracted from 0.22 μm-filter-concentrated groundwaters from BA1A and BA1D . Read relative abundances are reported as percentages rounded to the ones place. Cases when a taxon was detected in a sample and was $<$ 1 % read relative abundance after rounding are labeled "$<$ 1". Cases when no reads of a taxon were detected in a sample, but when that taxon was detected in 16S gene reads of other Oman samples obtained during the same sampling year, are labeled "n.r." Cases when no reads were detected in any Oman sample within the data set of a given year are blank.

manuscript submitted to *JGR: Biogeosciences*

detected in sediments at radionuclide-contaminated sites (Lin et al., 2012) and in high-altitude, cold fumarolic environments (Costello et al., 2009), suggesting that members of GAL15 are stress-tolerant. Members of GAL15 were found to be more abundant in oxic than anoxic zones of a profile of sediment cores (Lin et al., 2012), suggesting that some members of GAL15 are tolerant of oxic conditions. However, our finding of a high relative abundance of GAL15-affiliated 16S rRNA gene reads in a sample of strongly reduced waters ($-412\,\mathrm{mV}$ *Eh* and $3.55\,\mu\mathrm{mol}\cdot\mathrm{L}^{-1}$ H_2; Tables 1 and 3) pumped from an isolated depth interval of 102 m to 132 m in a peridotite aquifer suggests that some members of GAL15 are anaerobes.

16S rRNA gene sequences were searched for matches to known CH_4-cycling taxa, as compiled previously (Crespo-Medina et al., 2017; Nothaft et al., 2020). Sequences closely affiliated with both methanogenic and aerobic methanotrophic taxa were found in multiple samples, but always in low relative abundance ($< 1\,\%$ of reads; Figure S6). These included sequences related to the genus *Methanobacterium*, whose members can produce CH_4 from H_2 and CO_2, CO, or formate (Balch et al., 1979) and are widespread in Samail Ophiolite groundwaters (Miller et al., 2016; Rempfert et al., 2017; Fones et al., 2019; Nothaft et al., 2020; Fones et al., 2020). In addition, relatives of aerobic methanotrophs of the genus *Methylocaldum* (Hanson & Hanson, 1996) and the family Methylacidiphilaceae (Op den Camp et al., 2009) were detected.

Previous studies have shown that organisms inhabiting environments that impose stress often exhibit smaller cells sizes (Luef et al., 2015). To explore whether this phenomenon is also true in the Samail Ophiolite, biomass was collected sequentially onto filters with pore diameters of $0.45\,\mu$m, $0.22\,\mu$m, and $0.10\,\mu$m by connecting three inline filter housings in series when sampling BA1A in 2018 (Figure S7, Text S1, Figure S2). Microbial community compositions were similar across filters of different pore diameters (Figure S7), with the exception of relatives of the genus *Brachymonas*, which had highest relative abundance in the $0.10\,\mu$m pore-diameter filter in the sample from $> 100\,\mathrm{m}$ depth (80 % of reads, compared to 9 % to 10 % in filters of other pore diameters), but showed decreased relative read abundance with decreasing pore size in samples of the 55 m to 66 m depth interval (44 %, 32 %, and 26 % in the $0.45\,\mu$m, $0.22\,\mu$m, and $0.10\,\mu$m pore-diameter filters, respectively). Although a greater sample size would be required to robustly interpret trends of microbial community composition as a function of cell size in this environment, our ability to extract and sequence DNA from cells between $0.22\,\mu$m and $0.10\,\mu$m in diameter is in itself notable because streamlining (shrinking) of cell and/or genome sizes has been proposed as an adaptive strategy to reduce the energetic costs of replication under conditions of environmental stress (Giovannoni et al., 2014), including the challenging conditions of high pH and low electron acceptor and inorganic C availability found in parts of the Samail Ophiolite (Suzuki et al., 2017; Fones et al., 2019).

In addition to biomass samples obtained during pumping, a sample of drill foam/fluid was taken as it emerged from BA1A during drilling in order to evaluate potential contamination of the subsurface with exogenous microbes. The most abundant 16S rRNA gene sequences in the drill foam/fluid sample were distinct from those of samples obtained during subsequent groundwater pumping (Figure S8, Text S1). This suggests that most of the taxa identified in samples subsequently obtained from pumping groundwaters from the subsurface were not derived from drill fluids.

5 Discussion

5.1 Sources and mixing of groundwaters

To derive an integrated hydrologic and geochemical conceptual model of the BA1A/BA1D system, we revisit the trends in the wireline logs and pumped sample geochemistry in light of the physical hydrological conclusions of Lods et al. (2020) (Section 3). In the case

of BA1A, where downward flow within the borehole under ambient conditions has been recorded (Section 3), it appears that the wireline log pH, Eh, and electrical conductivity trends (Figure 1; Section 4.1) reflect displacement of moderately alkaline water from the surficial (< 27 m) aquifer down to depths approaching 200 m, where it mixes in the borehole with hyperalkaline $Ca^{2+}-OH^-$ waters from deeper aquifers. In contrast, pumped samples of packed intervals at depths ≥ 100 m in BA1A drew water from the surrounding rock formations that was more hyperalkaline and reduced (Table 1) than in the open borehole at the same depth. In BA1D, where no ambient flow within the borehole was recorded (Section 3), the well logs and pumped samples show closer agreement. Thus, differences in logs and pumped sample chemical compositions in BA1A and BA1D may result from variable within-borehole flow regimes. We speculate that, prior to drilling, the 41 m to 75 m aquifer near BA1A may have been reduced and hyperalkaline, as BA1D was in that depth interval during sampling in 2019, and that the strong drilling-induced connection of the surficial (< 27 m) aquifer to the 41 m to 75 m aquifer through the BA1A borehole resulted in the oxidized and moderately alkaline compositions recorded in our samples of BA1A at depths < 70 m (Table 1).

The $\sum$Si and pH data provide further insights into aquifer dynamics. Although the aquifers are nominally in dunite, the pH of $Ca^{2+} - OH^-$ waters ($\geq$ 10.67; Table 1) indicates that they must have reacted with diopside along their flow paths. Reaction of water with Mg-endmember olivine (forsterite) alone will reach chrysotile-brucite equilibrium at pH $\sim$ 10 (Leong & Shock, 2020). The addition of enstatite is also insufficient to increase pH past 11. Rather, pH exceeds 11 only when diopside is present (Leong & Shock, 2020). Thus, there may be some small amount of diopside within the dunites, or the waters may have sourced from outside of the immediate, dunitic surroundings of the boreholes. Both are possible because small amounts of diopside are common in Oman dunites (P. B. Kelemen et al., 1995), and harzburgites are present throughout the catchment where BA1A and BA1D are situated.

The indication that these waters have reacted with olivine and diopside validates the use of the Leong et al. (2020) Si mixing model. Our samples plot close to the mixing line associated with the 20 μmol·kg^{-1} $c_{\sum \mathrm{CO_2}}$ chrysotile-brucite-calcite end member of Leong et al. (2020) (leftmost dotted mixing line in Figure 2). Assuming this as a compositional end-member, the extent of mixing with a $Mg^{2+} - HCO_3^-$ water endmember is shown in Figure 2 and tabulated in Table S1. These calculations reveal a trend of decreasing contribution of $Mg^{2+}-HCO_3^-$ water to the total water mass with increasing depth in BA1A. This is consistent with the hydrologic flowmeter tests that showed strong downflow in the upper 60 m at BA1 (Lods et al., 2020). At greater depths, ambient flow was below detection ($< 0.1\,\mathrm{L}\cdot\mathrm{min}^{-1}$), but appears to slowly influence the chemical composition of borehole waters to depths approaching 200 m, as evidenced by the wireline logs (Figure 1). Compared to BA1A, BA1D has lower calculated proportions of $Mg^{2+} - HCO_3^-$ water (only 2.8 % $Mg^{2+} - HCO_3^-$ in the 45 m to 75 m interval and 1.9 % $Mg^{2+} - HCO_3^-$ in the 102 m to 132 m interval; Table S1; Figure 2). This is consistent with the lack of evidence of downflow within BA1D. The collection of near end-member $Ca^{2+}-OH^-$ fluids from these deeper intervals in BA1D indicates that the packer system is a promising tool for retrieving end-member $Ca^{2+}-OH^-$ waters from deep ophiolite aquifers, even when these aquifers are overlain by aquifers containing $Mg^{2+}-HCO_3^-$ waters.

5.2 Dissolved gas dynamics

Before interpreting our gas chemistry results, the possibility of degassing during sampling must be addressed. Bubbles were observed in the pumped outflow when pumping the hyperalkaline intervals. In addition, interferences with in-line flow meter (Figure S2) readings were observed during pumping of BA1D in 2019, which were rectified by tilting the flow meter at an incline, suggesting that bubbles in the flow meter were

causing the unstable readings. These observations suggest that partial gas exsolution may have occured upstream of the flow-splitting manifold used for collecting our samples (Figure S2). A potential cause of degassing is cavitation associated with the fittings or measurement mechanisms of the flow meter.

That said, some simple calculations of tubing diameters and flow rates suggest that degassing probably had a minor effect on our data. The black tubing connecting from the pipe string outlet to the flow meter, and then downstream towards the flow-splitting manifold (Figure S2), had a diameter of $\sim$ 2.5 cm and a length of $\sim$ 10 m. Given our typical flow rates of 20 $L \cdot min^{-1}$, the residence time of water in this tubing was 15 s, suggesting that kinetics of exsolution would have limited degassing over the short time period between fluids exiting the pipe string and arriving at the gas sampling apparatus. Further, noting that packed intervals were generally pumped for an hour or more prior to geochemical sampling, more than 200 tubing-volumes of water were pumped through the tubing prior to sampling (assuming flow of 20 $L \cdot min^{-1}$ for 60 min). This suggests that, if gas bubbles were present at some locations within the sampling tubing or flow meter, they would have had time to approach equilibrium with gases in the pumped waters, resulting in gas partial pressures in the sampled fluids approaching those of the fluids in the pumped interval. Thus, while we cannot strictly rule out that degassing affected our measured gas concentrations and isotopic compositions, these calculations suggest that our data are likely representative and informative. Still, the gas concentrations reported here should be considered minimum values until future work in which gas samples are taken closer to the wellhead at BA1A and BA1D corroborates our results.

The concentration of H_2 at BA1A and BA1D, which ranged up to 4 $\mu mol \cdot L^{-1}$ (Table 3), is modest in comparison to other hyperalkaline waters in the ophiolite. Well NSHQ14, which is located 2 km down-gradient within the same catchment as BA1A and BA1D, hosts waters of pH $\sim$ 11.4 with at least two orders of magnitude higher c_{H_2} (A. Paukert, 2014; Nothaft et al., 2020) than the maximum c_{H_2} observed at BA1A and BA1D. These differences could stem from variations in reaction extent and/or lithology between the two wells. In addition, microbial H_2 consumption, notably coupled to SO_4^{2-} reduction (Section 4.3), could decrease c_{H_2} at BA1A and BA1D.

The high $\delta^{13}C$ value of C_2H_6 (-2.5 ‰ VPDB; Table 4; Figure 4) in sample BA1D_2019_102-132 indicates an abiotic source of C_2H_6, which has also been proposed for C_2H_6 elsewhere in the ophiolite (Fritz et al., 1992; Nothaft et al., 2020). If C_2H_6 is indeed abiotic at BA1D, then at least some of the CH_4 at BA1A and BA1D is likely also abiotic. However, the detection of 16S rRNA gene sequences affiliated with methanogens of the genus *Methanobacterium* at BA1A and BA1D, albeit in low abundances (< 1 % of reads; Section 4.3; Figure S6), suggests a potential additional contribution of microbial CH_4.

Perhaps the most remarkable aspect of our gas data is the ^{13}C and D enrichment of CH_4, particularly in sample BA1A_2019_108-132 (23.9 ‰ VPDB and 45 ‰ VSMOW; Table 4). This isotopic composition on its own, and especially compared to the relatively less ^{13}C- and D-enriched (but still quite enriched) samples from BA1D (Figure 3), is hard to explain without invoking microbial CH_4 oxidation (Section 4.2). This inference is further supported by the lower c_{CH_4} and C_1/C_2 ratio of BA1A_2019_108-132 relative to the BA1D samples (Table 3; Figure S3). CH_4 samples from BA1D may have also undergone microbial oxidation to lesser extents.

5.3 Microbial ecology

As proposed in Section 5.1, hydrologic and geochemical data indicate that the 41 m to 75 m aquifer at BA1A may have been hyperalkaline and reduced prior to drilling, similar to the geochemical state of BA1D in 2019 at equivalent depths. If this is so, we infer that, prior to drilling, BA1A and BA1D below $\sim$ 40 m hosted a microbial ecosystem dominated by SO_4^{2-} reduction coupled to oxidation of H_2 and/or organic C such as

the μmol $\cdot$ L^{-1} concentrations of small molecular weight compounds such as formate, acetate etc. commonly detected in Samail Ophiolite fluids (Rempfert et al., 2017). Ongoing SO_4^{2-} reduction is consistent with the sulfidic smell observed during drilling of BA1A. The high relative 16S rRNA gene abundance (up to 92 % of reads) of sequences related to Thermodesulfovibriona, particularly in BA1D and in OM19_BA1A_108_132, suggest that SO_4^{2-} reduction likely continues to be an important microbial process in much of the subsurface intersected by BA1A and BA1D, particularly in the more reduced zones. Metagenome-assembled genomes affiliated with genus *Thermodesulfovibrio* within Thermodesulfovibrionia suggest that *Thermodesulfovibrio* is widespread in the Samail Ophiolite and is not capable of CO_2 fixation (Templeton et al., this issue). As such, this *Thermodesulfovibrio* population engages in chemolithoheterotrophy, which is an uncommon metabolic strategy but one observed in several archaeal cultivars (Amenabar et al., 2018). This metabolic strategy may be particularly well-suited to $\sum CO_2$-depleted, hyperalkaline conditions, so long as there is a steady source of organic C. Bioenergetic, metagenomic, and metatranscriptomic evidence of bacterial SO_4^{2-} reduction has also been found at other sites of serpentinization such as the Coast Range Ophiolite (Sabuda et al., 2020) and the Lost City Hydrothermal Vent Field, Mid-Atlantic ridge (Lang et al., 2018). Moreover, low but detectable rates of microbial SO_4^{2-} reduction have been measured in groundwaters sampled from wells in the Samail Ophiolite and the Coast Range Ophiolite (Glombitza et al., in revision). In addition, there was notable blackening and sulfurization of the drill chips recovered during BA1A drilling and analyzed by optical and Raman spectroscopy (E. Ellison and A. Templeton, personal communication, 2020), which could have been caused by reaction with sulfidic fluids.

The source of the nearly mmol$\cdot L^{-1}$ levels SO_4^{2-} at BA1D is unclear. One explanation is leaching of SO_4^{2-} salts previously loaded into these rocks during partial serpentinization during near-spreading ridge hydrothermal alteration and/or during obduction. Another is the oxidation of reduced S in the rocks, which can occur either abiotically or biotically during weathering processes in the presence of O_2 or NO_3^- (Luther et al., 2011). The reduced sulfur may source from more S-rich gabbros, which are present in intrusive dikes at the BA1 wells, or from sulfide minerals, which are pervasive in partially altered peridotites in the BA1 wells (Lods et al., 2020; P. Kelemen et al., 2020).

S-oxidizing bacteria including relatives of the genera *Sulfuritalea* and *Cupriavidus*, as well as the family Rhodocyclaceae, have accounted for particularly high relative abundances of 16S rRNA gene reads in groundwaters sampled from wells in the Samail Ophiolite that show evidence of mixing of reduced, hyperalkaline waters with more oxidized $Mg^{2+}-HCO_3^-$ waters and/or gabbro-reacted waters, suggesting that microbial S oxidation occurs at redox interfaces and mixing zones in the ophiolite (Rempfert et al., 2017). In searching the BA1A and BA1D 16S rRNA gene sequences for the S-oxidizing bacteria noted by Rempfert et al. (2017), sequences related to Rhodocyclaceae and *Cupriavidus* were found at up to 2 % of reads at BA1A, indicating that microbial S-oxidizing processes may occur at BA1A, although the extent of these processes may be minor. We also note that the DrillFoam used in drilling (Section 2.1) is a biodegradable, sulfate-containing compound, so this may have been an additional source of SO_4^{2-} to the system, although it is not necessary to invoke this biodegradation process as the source of SO_4^{2-}, given the presence of the natural S reservoirs discussed above.

In addition to SO_4^{2-} reduction coupled to H_2 oxidation, secondary anaerobic, autotrophic processes at BA1A and BA1D may include hydrogenotrophic methanogenesis, evidenced by the presence of 16S rRNA genes affiliated with genus *Methanobacterium* in < 1 % of reads (Figure S6; Section 4.3), and homoacetogenesis, evidenced by the presence of 16S rRNA genes affiliated with putative acetogens of the class *Acetothermiia* ((Takami et al., 2012)) in up to 2 % of reads (Figure 5). The apparent dominance of SO_4^{2-} reduction over methanogenesis at BA1A and BA1D presents an interesting contrast to the relative influences of these processes at the nearby (2 km away) and more H_2-rich (10^2 μmol$\cdot$

712 L^{-1} to $10^3\,\mu mol \cdot L^{-1}$; (A. Paukert, 2014; Nothaft et al., 2020)) well NSHQ14, where
713 the abundance and activity of methanogens is comparable to, if not substantially greater
714 than, that of SO_4^{2-} reducers (Miller et al., 2016; Rempfert et al., 2017; Fones et al., 2019;
715 Nothaft et al., 2020; Fones et al., 2020; Kraus et al., 2021). This implies the potential
716 existence of a threshold level of production of reduced compounds, such as H_2 or formate
717 ($HCOO^-$), in continental, low-temperature serpentinizing settings, at which methano-
718 genesis becomes energetically competitive with SO_4^{2-} reduction. The juxtaposition of
719 the BA1 wells vs. NSHQ14 suggests that this transition may occur at H_2 concentrations
720 in the range of $10\,\mu mol \cdot L^{-1}$ to $10^2\,\mu mol \cdot L^{-1}$ in the Samail Ophiolite. Such a transi-
721 tion has been described in sedimentary settings, but at orders of magnitude lower c_{H_2}
722 ($\sim 5\,nmol \cdot L^{-1}$; (Lovley et al., 1994; Kampbell et al., 1998)). The higher apparent c_{H_2}
723 threshold in serpentinizing settings such as the Samail Ophiolite may be a consequence
724 of the stressors of high pH and low CO_2 availability unique to serpentinizing settings.
725 At hyperalkaline conditions, microbes must expend additional energy to regulate cyto-
726 plasmic pH and to maintain a proton motive force across the cell membrane to gener-
727 ate ATP (Mitchell, 2011; Mulkidjanian et al., 2008). High pH has been shown to be more
728 important than substrate availability in limiting microbial SO_4^{2-} reduction rates in serpentinization-
729 influenced waters from the Samail Ophiolite and the Coast Range Ophiolite (Glombitza
730 et al., 2019). One might expect high pH to be an even greater burden for hydrogenotrophic
731 methanogens due to their reliance on CO_2 for both C fixation and as an oxidant in their
732 energy metabolism. Thus, a higher c_{H_2} threshold for competition between SO_4^{2-} reduc-
733 ers and methanogens in serpentinizing settings relative to sedimentary settings may re-
734 sult from the high pH and related geochemical challenges.

735 Our detection of high relative abundances of 16S rRNA genes related to heterotrophic
736 bacteria capable of respiration using O_2 or NO_3^-, such as *Brachymonas* and *P. lavamen-*
737 *tivorans*, in samples of BA1A taken from $< 70\,m$ depth (Figure 5; Section 4.3), taken
738 together with the trends of decreasing $c_{NO_3^-}$ with increasing depth at BA1A (Section 4.1),
739 suggest that heterotrophic, aerobic and/or denitrifying microbial metabolisms may be
740 active in shallow, subsurface regions. *Brachymonas* and *P. lavamentivorans* have been
741 detected in 16S rRNA gene surveys of the Samail Ophiolite prior to Oman Drilling Project
742 activities in low relative abundance (typically $< 1\,\%$ of reads and not exceeding $6\,\%$; (Miller
743 et al., 2016; Rempfert et al., 2017; Nothaft et al., 2020; Kraus et al., 2021)), but these
744 taxa were not detected in samples of the drilling fluids used at BA1A (Sections 4.3 and
745 S1; Figure S8). This suggests that these taxa are native to the Samail Ophiolite rather
746 than exogenous drilling contaminants. Natural *Brachymonas* and *P. lavamentivorans*
747 populations may have bloomed in response to an influx of oxidized water at depth when
748 previously separated aquifers at different depths were connected by drilling at BA1A (Sec-
749 tion 3). Interestingly, *P. lavamentivorans* has been noted for its ability to degrade syn-
750 thetic laundry surfactants (Schleheck et al., 2011), suggesting that it could have partic-
751 ipated in the biodegradation of DrillFoam (Section 2.1) introduced into the aquifer dur-
752 ing drilling.

753 As discussed in Sections 4.2 and 5.2, there is strong isotopic evidence of microbial
754 CH_4 oxidation in fluids accessed by both wells, and especially at BA1A (Figure 3). A
755 search of 16S rRNA gene sequences related to cultured CH_4 oxidizers yielded few matches
756 at BA1A ($< 1\,\%$ of reads) and none at BA1D. Also, all matches are related to Bacte-
757 ria thought to exclusively use O_2 to oxidize CH_4 (Figure S6; Section 4.3). It is possible
758 that microbial CH_4 oxidizers are rare at BA1A and BA1D, particularly compared to dom-
759 inant taxa such as Thermodesulfovibrionia. CH_4 oxidation may be a minor process that
760 could have been briefly stimulated by O_2 influx during drilling. Alternatively, there may
761 be organisms at BA1A and BA1D whose capacity to oxidize CH_4 under anaerobic con-
762 ditions has not yet been documented. Future work could employ shotgun metagenomic
763 sequencing to generate a database of genes to examine for those related to CH_4 oxida-
764 tion (e.g., *pmoA* for aerobic methanotrophs, *mcrA* for anaerobic methanotrophs). Al-
765 ternatively, microcosm assays or enrichment cultures from BA1A and BA1D that are amended

with CH_4 and one of several oxidants (e.g., O_2, SO_4^{2-}) could be used to detect activity and/or identify microbes with CH_4 oxidation capabilities.

5.4 Isotopic composition of $\sum CO_2$

Ophiolitic $Mg^{2+}-HCO_3^-$ waters are in open-system communication with the atmosphere (Neal & Stanger, 1985; Bruni et al., 2002; Cipolli et al., 2004; A. N. Paukert et al., 2012; Leong & Shock, 2020). This is also true of seawater, which sets the $\delta^{13}C$ of seawater $\sum CO_2$ at 0 ‰ VPDB to 2 ‰ VPDB, reflecting a series of isotopic equilibria connecting HCO_3^-, the dominant $\sum CO_2$ species in seawater, to the isotopic composition of atmospheric CO_2 (Zeebe & Wolf-Gladrow, 2001). Yet, the $\delta^{13}C$ values of $\sum CO_2$ in the $Mg^{2+}-HCO_3^-$ waters in the upper 70 m of BA1A (Table 4; Section 4.2) and in other $Mg^{2+}-HCO_3^-$ waters pumped from wells in the ophiolite (Matter et al., 2006; Nothaft et al., 2020) are ~ 15 ‰ lower than that of marine $\sum CO_2$. This discrepancy raises the question of whether equilibrium with atmospheric CO_2 is the only factor affecting $\sum CO_2$ in ophiolitic $Mg^{2+} - HCO_3^-$ waters.

In freshwater systems, respiration of organic matter in soils can be an important factor affecting $\delta^{13}C_{\sum CO_2}$ (Waldron et al., 2007). However, vegetation and soil cover are sparse in the Samail Ophiolite (Figure S1), so it may not be valid to assume that respiration in soils has the capacity to affect $\delta^{13}C_{\sum CO_2}$ to the extent that is observed. However, organic C within the crystalline bedrock may be oxidized by microbes, thereby producing ^{13}C-depleted $\sum CO_2$. Total organic C in peridotites exposed to alteration at the seafloor, a proxy for organic C endogenous to the Samail Ophiolite, is relatively ^{13}C-depleted (approximately -25 ± 5 ‰ VPDB; (Alt et al., 2013; Alt, Garrido, et al., 2012; Alt, Shanks, et al., 2012; Delacour et al., 2008)). CH_4 in fluid inclusions (Kelley, 1996; Kelley & Früh-Green, 1999; Miura et al., 2011; Klein et al., 2019; Grozeva et al., 2020) is another potential source of reduced C. Microbial respiration of these endogenous sources of reduced C could decrease $\delta^{13}C_{\sum CO_2}$ below equilibrium with atmospheric CO_2 if this respiration occurs at rates comparable to or faster than air-water CO_2 exchange.

This hypothesis should be testable by measuring the ^{14}C content of $\sum CO_2$ in $Mg^{2+}-HCO_3^-$ waters waters. To our knowledge, there is only one such analysis in the literature on the Samail Ophiolite. This is from well WDA17, which is situated in peridodite, has a groundwater pH of 9.10, $c_{\sum CO_2}$ of 2.481 mmol·kg^{-1}, $\delta^{13}C_{\sum CO_2}$ of -12.3 ‰ VPDB, $F^{14}C_{\sum CO_2}$ of 0.205 (corresponding to a ^{14}C age of 12 700 years B.P.), and a $^3H/^3He$ recharge age of 21.5 years (Paukert Vankeuren et al., 2019). It is interesting that the ^{14}C "age" of the $\sum CO_2$ in this sample is considerably older than its $^3H/^3He$-derived recharge age and that its $\delta^{13}C_{\sum CO_2}$ is well below that which would be expected based on carbonate equilibrium with atmospheric CO_2. These characteristics are compatible with the hypothesis of recent microbial oxidation of ancient organic matter stored in the partially-serpentinized peridotites.

An alternative explanation would be that the ^{14}C-free C derives from dissolution/reprecipitation of carbonate veins that are ^{14}C-free. Such veins could have inherited C from marine organic C through thermochemical sulfate reduction (Goldstein & Aizenshtat, 1994), which can produce relatively ^{13}C-depleted inorganic C. However, this suggestion is complicated by the fact that calcite, dolomite, and magnesite are typically at or above saturation in $Mg^{2+}-HCO_3^-$ waters in the Samail Ophiolite (Neal & Stanger, 1985; Matter et al., 2006), and magnesite should precipitate (rather than dissolve) from these waters during reaction with peridotite (Bruni et al., 2002; A. N. Paukert et al., 2012).

The ^{13}C depletion of $\sum CO_2$ below equilibrium with atmospheric CO_2 in $Mg^{2+}-HCO_3^-$ waters could alternatively be explained by these waters expressing a muted signal of the kinetic isotope effects associated with hydroxylation of aqueous CO_2, which have been invoked to explain the stark ^{13}C depletion in Ca-rich carbonate travertine de-

posits found at hyperalkaline springs in ophiolites (Clark & Fontes, 1990; Clark et al., 1992; P. B. Kelemen et al., 2011; Falk et al., 2016). However, this seems unlikely because a rapid CO_2 uptake process would be necessary to achieve these kinetic isotopic effects. Further, in contrast to the travertine deposits, there is no clear mechanism to preserve such a signature in a $Mg^{2+}-HCO_3^-$ water (as in a precipitation process), so CO_2 (aq) and HCO_3^- would be expected to quickly re-equilibrate.

Although we cannot resolve the compositional and isotopic dynamics of inorganic C in $Mg^{2+}-HCO_3^-$ waters given the available data, this discussion has highlighted important aspects of the C cycle of low-temperature serpentinizing systems that are ripe for future investigation. Further analyses of the stable and radio isotopic compositions of inorganic C in ophiolitic $Mg^{2+}-HCO_3^-$ waters, especially if coupled to $^3H/^3He$-derived recharge ages, could advance understanding of the timescales and sources of CO_2 uptake in near-surface serpentinizing aquifers.

6 Conclusions

In this study, vertically- and horizontally-resolved sample acquisition via the deployment of a packer system in two 400 m-deep wells enabled a holistic geochemical, hydrologic, and biological investigation into an aquifer experiencing ongoing low-temperature serpentinization. In addition, a temporal component was assessed by monitoring subsurface biogeochemical states from the time of well completion to three years afterwards. Through the isolation and pumping of discrete intervals as deep as 108 m to 132 m below ground level, we interrogated how microbial communities of minimally-disturbed, hyperalkaline, and reduced groundwaters differed from those of pervasively mixed and oxidized groundwaters. Aqueous chemical analyses and 16S rRNA gene sequencing of deep, $Ca^{2+}-OH^-$ groundwaters revealed the presence of a microbial ecosystem dominated by organisms potentially supported by H_2 oxidation coupled to SO_4^{2-} reduction, with small organic acids generated through sesrpentinization possibly serving as an organic C source. Based on these findings, we propose that future investigations of the borehole lithology seek evidence for late-stage sulfurization induced by microbial activity. In oxidized $Mg^{2+}-HCO_3^-$ groundwaters, heterotrophic bacterial aerobes and/or denitrifiers were dominant. This may be a common state for the shallow aquifers, or it may have been stimulated by drilling-induced groundwater mixing. Isotopic data point to intriguing future avenues of C cycle investigations in this system. Stark ^{13}C and D enrichments in CH_4 and ^{13}C depletions in $\sum CO_2$ of $Mg^{2+}-HCO_3^-$ groundwaters below the expectation of equilibrium with atmospheric CO_2 suggest the importance of cryptic microbial oxidation of stored C reservoirs. Overall, the methodology and results of this study mark an important step towards an integrated hydrologic and biogeochemical understanding of the serpentinite-hosted biosphere. As such, this study presents a framework for exploring where subsurface energy availability is greatest and how that maps onto microbial abundance and activity, information that is needed for improving strategies for life detection in fractured rock aquifers on and beyond Earth.

7 Acknowledgements

This research was directly supported by the Rock-Powered Life NASA Astrobiology Institute (NNA15BB02A; Principal Investigator (PI): Alexis Templeton). This research also used samples and/or data provided by the Oman Drilling Project. The Oman Drilling Project (OmanDP) has been possible through co-mingled funds from the International Continental Scientific Drilling Project (ICDP; lead PIs: Peter Kelemen, Juerg Matter, and Damon Teagle), the Sloan Foundation – Deep Carbon Observatory (Grant 2014-3-01; PI: Peter Kelemen), the National Science Foundation (NSF-EAR-1516300; PI: Peter Kelemen), the NASA Astrobiology Institute (NNA15BB02A; PI: Alexis Templeton), the German Research Foundation (DFG; PI: Jrgen Koepke), the Japanese So-

ciety for the Promotion of Science (JSPS; PI: Katsuyoshi Michibayashi), the European Research Council (PI: Bjorn Jamtveit), the Swiss National Science Foundation (PI: Gretchen Frh-Green), JAMSTEC, the TAMU-JR Science operator, and in kind contributions from the Sultanate of Oman Ministry of Regional Municipalities and Water Resources, the Oman Public Authority of Mining, Sultan Qaboos University, CNRS-Universit Montpellier II, Columbia University, and the University of Southampton.

We thank the Ministry of Regional Municipalities and Water Resources in the Sultanate of Oman (particularly Said Al Habsi, Rashid Al Abri, Salim Al Khanbashi, and Haider Ahmed Mohammed Alajmi) for allowing access to wells and logistical support, Zaher Al Sulaimani and Mazin Al Sulaimani from the Oman Water Centre and AZD Engineering for their technical and logistical support, Jude Coggon for coordinating Oman Drilling Project activities, Nehal Warsi for overseeing curation of all OmanDP cores, Eric Ellison for performing Si analyses, Elizabeth Fones for preparing samples for DNA sequencing, James Leong and Emily Kraus for sharing data, and Peter Kelemen for helpful comments on the manuscript.

Data (in Excel format) and source code (in R Markdown format) used to produce the figures, data tables and analyses for this paper (as well as additional data on analytical uncertainties and trace element concentrations) are available online at `https://github.com/danote/Oman-packers-2018-2019`. Additional DNA sequence data processing codes are available at `https://github.com/danote/Samail_16S_compilation`.

References

Abrajano, T., Sturchio, N., Kennedy, B., Lyon, G., Muehlenbachs, K., & Bohlke, J. (1990). Geochemistry of reduced gas related to serpentinization of the Zambales ophiolite, Philippines. *Appl. Geochem.*, *5*(5), 625 - 630. Retrieved from `http://www.sciencedirect.com/science/article/pii/088329279090060I` (Water-Rock Interactions Special Memorial Issue Ivan Barnes (1931–1989)) doi: 10.1016/0883-2927(90)90060-I

Alt, J. C., Garrido, C. J., Shanks, W., Turchyn, A., Padrón-Navarta, J. A., Sánchez-Vizcaíno, V. L., ... Marchesi, C. (2012). Recycling of water, carbon, and sulfur during subduction of serpentinites: A stable isotope study of Cerro del Almirez, Spain. *Earth Planet. Sci. Lett.*, *327-328*, 50 - 60. Retrieved from `http://www.sciencedirect.com/science/article/pii/S0012821X12000568` doi: 10.1016/j.epsl.2012.01.029

Alt, J. C., Schwarzenbach, E. M., Früh-Green, G. L., Shanks, W. C., Bernasconi, S. M., Garrido, C. J., ... Marchesi, C. (2013). The role of serpentinites in cycling of carbon and sulfur: Seafloor serpentinization and subduction metamorphism. *Lithos*, *178*, 40 - 54. Retrieved from `http://www.sciencedirect.com/science/article/pii/S0024493712004975` (Serpentinites from mid-oceanic ridges to subduction) doi: 10.1016/j.lithos.2012.12.006

Alt, J. C., Shanks, W., Crispini, L., Gaggero, L., Schwarzenbach, E. M., Früh-Green, G. L., & Bernasconi, S. M. (2012). Uptake of carbon and sulfur during seafloor serpentinization and the effects of subduction metamorphism in Ligurian peridotites. *Chem. Geol.*, *322-323*, 268 - 277. Retrieved from `http://www.sciencedirect.com/science/article/pii/S0009254112003154` doi: 10.1016/j.chemgeo.2012.07.009

Amenabar, M. J., Colman, D. R., Poudel, S., Roden, E. E., & Boyd, E. S. (2018). Electron acceptor availability alters carbon and energy metabolism in a thermoacidophile. *Environ. Microbiol.*, *20*(7), 2523-2537. Retrieved from `https://sfamjournals.onlinelibrary.wiley.com/doi/abs/10.1111/1462-2920.14270` doi: 10.1111/1462-2920.14270

ASTM. (2016). *Astm d859-16, standard test method for silica in water* (Tech. Rep.). ASTM International. doi: 10.1520/D0859-16

Balch, W. E., Fox, G. E., Magrum, L. J., Woese, C. R., & Wolfe, R. S. (1979, Jun). Methanogens: reevaluation of a unique biological group. *Microbiol. Rev.*, *43*(2), 260. Retrieved from https://www.ncbi.nlm.nih.gov/pmc/articles/PMC281474

Barnes, I., LaMarche, j. V., & Himmelberg, G. (1967). Geochemical evidence of present-day serpentinization. *Science*, *156*(3776), 830–832. doi: 10.1126/science.156.3776.830

Barnes, I., & O'Neil, J. R. (1969). The relationship between fluids in some fresh alpine-type ultramafics and possible modern serpentinization, western United States. *Geol. Soc. Am. Bull.*, *80*(10), 1947–1960. doi: 10.1130/0016-7606(1969)80[1947:TRBFIS]2.0.CO;2

Blöthe, M., & Roden, E. E. (2009). Composition and Activity of an Autotrophic Fe(II)-Oxidizing, Nitrate-Reducing Enrichment Culture. *Appl. Environ. Microbiol.*, *75*(21), 6937–6940. Retrieved from https://aem.asm.org/content/75/21/6937 doi: 10.1128/AEM.01742-09

Boronina, A., Renard, P., Balderer, W., & Christodoulides, A. (2003). Groundwater resources in the Kouris catchment (Cyprus): data analysis and numerical modelling. *J. Hydro.*, *271*(1), 130-149. Retrieved from https://www.sciencedirect.com/science/article/pii/S0022169402003220 doi: 10.1016/S0022-1694(02)00322-0

Boulart, C., Chavagnac, V., Monnin, C., Delacour, A., Ceuleneer, G., & Hoareau, G. (2013). Differences in gas venting from ultramafic-hosted warm springs: the example of Oman and Voltri ophiolites. *Ofioliti*, *38*(2), 142–156. doi: 10.4454/ofioliti.v38i2.423

Brazelton, W., Nelson, B., & Schrenk, M. (2012). Metagenomic Evidence for H_2 Oxidation and H_2 Production by Serpentinite-Hosted Subsurface Microbial Communities. *Front. Microb.*, *2*, 268. Retrieved from https://www.frontiersin.org/article/10.3389/fmicb.2011.00268 doi: 10.3389/fmicb.2011.00268

Brazelton, W. J., Thornton, C. N., Hyer, A., Twing, K. I., Longino, A. A., Lang, S. Q., ... Schrenk, M. O. (2017). Metagenomic identification of active methanogens and methanotrophs in serpentinite springs of the Voltri Massif, Italy. *PeerJ*, *5*, e2945. doi: 10.7717/peerj.2945

Brewer, T. E., Aronson, E. L., Arogyaswamy, K., Billings, S. A., Botthoff, J. K., Campbell, A. N., ... Fierer, N. (2019). Ecological and Genomic Attributes of Novel Bacterial Taxa That Thrive in Subsurface Soil Horizons. *mBio*, *10*(5). Retrieved from https://mbio.asm.org/content/10/5/e01318-19 doi: 10.1128/mBio.01318-19

Bruni, J., Canepa, M., Chiodini, G., Cioni, R., Cipolli, F., Longinelli, A., ... Zuccolini, M. V. (2002). Irreversible water–rock mass transfer accompanying the generation of the neutral, Mg–HCO3 and high-pH, Ca–OH spring waters of the Genova province, Italy. *Appl. Geochem.*, *17*(4), 455–474. doi: 10.1016/S0883-2927(01)00113-5

Callahan, B. J., McMurdie, P. J., Rosen, M. J., Han, A. W., Johnson, A. J. A., & Holmes, S. P. (2016, May). DADA2: High-resolution sample inference from Illumina amplicon data. *Nat. Methods*, *13*(7), 581. doi: 10.1038/nmeth.3869

Canovas III, P. A., Hoehler, T., & Shock, E. L. (2017). Geochemical bioenergetics during low-temperature serpentinization: An example from the Samail ophiolite, Sultanate of Oman. *J. Geophys. Res.: Biogeosci.*, *122*(7), 1821–1847. doi: 10.1002/2017JG003825

Chavagnac, V., Ceuleneer, G., Monnin, C., Lansac, B., Hoareau, G., & Boulart, C. (2013). Mineralogical assemblages forming at hyperalkaline warm springs hosted on ultramafic rocks: A case study of Oman and Ligurian ophiolites. *Geochem., Geophys., Geosyst.*, *14*(7), 2474-2495. Retrieved from https://agupubs.onlinelibrary.wiley.com/doi/abs/10.1002/ggge.20146

doi: 10.1002/ggge.20146

Chavagnac, V., Monnin, C., Ceuleneer, G., Boulart, C., & Hoareau, G. (2013). Characterization of hyperalkaline fluids produced by low-temperature serpentinization of mantle peridotites in the Oman and Ligurian ophiolites. *Geochem., Geophys., Geosyst.*, *14*(7), 2496–2522. doi: 10.1002/ggge.20147

Cipolli, F., Gambardella, B., Marini, L., Ottonello, G., & Zuccolini, M. V. (2004). Geochemistry of high-pH waters from serpentinites of the Gruppo di Voltri (Genova, Italy) and reaction path modeling of CO_2 sequestration in serpentinite aquifers. *Appl. Geochem.*, *19*(5), 787 - 802. Retrieved from `http://www.sciencedirect.com/science/article/pii/S0883292703002105` doi: 10.1016/j.apgeochem.2003.10.007

Clark, I. D., & Fontes, J.-C. (1990). Paleoclimatic Reconstruction in Northern Oman Based on Carbonates from Hyperalkaline Groundwaters. *Quat. Res.*, *33*(3), 320–336. doi: 10.1016/0033-5894(90)90059-T

Clark, I. D., Fontes, J.-C., & Fritz, P. (1992). Stable isotope disequilibria in travertine from high pH waters: Laboratory investigations and field observations from Oman. *Geochim. Cosmochim. Acta*, *56*(5), 2041 - 2050. Retrieved from `http://www.sciencedirect.com/science/article/pii/001670379290328G` doi: 10.1016/0016-7037(92)90328-G

Costello, E. K., Halloy, S. R. P., Reed, S. C., Sowell, P., & Schmidt, S. K. (2009). Fumarole-Supported Islands of Biodiversity within a Hyperarid, High-Elevation Landscape on Socompa Volcano, Puna de Atacama, Andes. *Appl. Environ. Microbiol.*, *75*(3), 735–747. Retrieved from `https://aem.asm.org/content/75/3/735` doi: 10.1128/AEM.01469-08

Crespo-Medina, M., Twing, K. I., Kubo, M. D. Y., Hoehler, T. M., Cardace, D., McCollom, T., & Schrenk, M. O. (2014). Insights into environmental controls on microbial communities in a continental serpentinite aquifer using a microcosm-based approach. *Front. Microb.*, *5*, 604. Retrieved from `https://www.frontiersin.org/article/10.3389/fmicb.2014.00604` doi: 10.3389/fmicb.2014.00604

Crespo-Medina, M., Twing, K. I., Sánchez-Murillo, R., Brazelton, W. J., McCollom, T. M., & Schrenk, M. O. (2017, May). Methane Dynamics in a Tropical Serpentinizing Environment: The Santa Elena Ophiolite, Costa Rica. *Front. Microb.*, *8*. Retrieved from `http://dx.doi.org/10.3389/fmicb.2017.00916` doi: 10.3389/fmicb.2017.00916

Delacour, A., Früh-Green, G. L., Bernasconi, S. M., Schaeffer, P., & Kelley, D. S. (2008). Carbon geochemistry of serpentinites in the Lost City Hydrothermal System (30 °N, MAR). *Geochim. Cosmochim. Acta*, *72*(15), 3681 - 3702. Retrieved from `http://www.sciencedirect.com/science/article/pii/S0016703708002585` doi: 10.1016/j.gca.2008.04.039

Dewandel, B., Lachassagne, P., Boudier, F., Al-Hattali, S., Ladouche, B., Pinault, J.-L., & Al-Suleimani, Z. (2005, 5). A conceptual hydrogeological model of ophiolite hard-rock aquifers in Oman based on a multiscale and a multidisciplinary approach. *Hydrogeol. J.*, *13*(5-6), 708–726. doi: 10.1007/s10040-005-0449-2

De Weert, J. P. A., Viñas, M., Grotenhuis, T., Rijnaarts, H. H. M., & Langenhoff, A. A. M. (2011, 02). Degradation of 4-n-nonylphenol under nitrate reducing conditions. *Biodegradation*, *22*(1), 175–187. Retrieved from `https://pubmed.ncbi.nlm.nih.gov/20640878` doi: 10.1007/s10532-010-9386-4

Etiope, G., Ifandi, E., Nazzari, M., Procesi, M., Tsikouras, B., Ventura, G., ... Szatmari, P. (2018, Jun). Widespread abiotic methane in chromitites. *Sci. Rep.*, *8*(1). Retrieved from `http://dx.doi.org/10.1038/s41598-018-27082-0` doi: 10.1038/s41598-018-27082-0

Etiope, G., Judas, J., & Whiticar, M. (2015). Occurrence of abiotic methane in the eastern United Arab Emirates ophiolite aquifer. *Arabian J. Geosci.*, *8*(12), 11345–11348. doi: 10.1007/s12517-015-1975-4

Falk, E., Guo, W., Paukert, A., Matter, J., Mervine, E., & Kelemen, P. (2016). Controls on the stable isotope compositions of travertine from hyperalkaline springs in Oman: Insights from clumped isotope measurements. *Geochim. Cosmochim. Acta*, *192*, 1 - 28. Retrieved from http://www.sciencedirect.com/science/article/pii/S0016703716303568 doi: 10.1016/j.gca.2016.06.026

Fones, E. M., Colman, D. R., Kraus, E. A., Nothaft, D. B., Poudel, S., Rempfert, K. R., ... Boyd, E. S. (2019). Physiological adaptations to serpentinization in the Samail Ophiolite, Oman. *ISME J.*, 1. doi: 10.1038/s41396-019-0391-2

Fones, E. M., Colman, D. R., Kraus, E. A., Stepanauskas, R., Templeton, A. S., Spear, J. R., & Boyd, E. S. (2020). Diversification of methanogens into hyperalkaline serpentinizing environments through adaptations to minimize oxidant limitation. *ISME J.*. Retrieved from https://doi.org/10.1038/s41396-020-00838-1 doi: 10.1038/s41396-020-00838-1

Frank, Y. A., Kadnikov, V. V., Lukina, A. P., Banks, D., Beletsky, A. V., Mardanov, A. V., ... Ravin, N. V. (2016). Characterization and Genome Analysis of the First Facultatively Alkaliphilic Thermodesulfovibrio Isolated from the Deep Terrestrial Subsurface. *Front. Microb.*, *7*, 2000. Retrieved from https://www.frontiersin.org/article/10.3389/fmicb.2016.02000 doi: 10.3389/fmicb.2016.02000

Fritz, P., Clark, I., Fontes, J.-C., Whiticar, M., & Faber, E. (1992). Deuterium and ^{13}C evidence for low temperature production of hydrogen and methane in a highly alkaline groundwater environment in Oman. In *International symposium on water-rock interaction* (Vol. 1, pp. 793–796). AA Balkema Rotterdam.

Giovannoni, S. J., Cameron Thrash, J., & Temperton, B. (2014). Implications of streamlining theory for microbial ecology. *ISME J.*, *8*(8), 1553–1565. Retrieved from https://doi.org/10.1038/ismej.2014.60 doi: 10.1038/ismej.2014.60

Glombitza, C., Kubo, M. D., Ellison, E. T., Rempfert, K. R., Matter, J. M., Templeton, A. S., & Hoehler, T. M. (2019, December). Microbial sulfate reduction rates in low temperature serpentinizing mantle rocks. In *Agu fall meeting abstracts* (Vol. 2019, p. B44C-06).

Glombitza, C., Putnam, L., Rempfert, K., Kubo, M., Schrenk, M., Templeton, & A.S., T., Hoehler. (in revision). Active microbial sulfate reduction in serpentinizing fluids of the continental subsurface. *Comm. Earth Environ.*.

Goldstein, T. P., & Aizenshtat, Z. (1994). Thermochemical sulfate reduction a review. *J. Therm. Anal.*, *42*(1), 241–290. Retrieved from https://doi.org/10.1007/BF02547004 doi: 10.1007/BF02547004

Grozeva, N. G., Klein, F., Seewald, J. S., & Sylva, S. P. (2020, FEB 21). Chemical and isotopic analyses of hydrocarbon-bearing fluid inclusions in olivine-rich rocks [Article]. *Philos. Trans. R. Soc., A*, *378*(2165, SI). doi: 10.1098/rsta.2018.0431

Habib, N., Khan, I. U., Hussain, F., Zhou, E.-M., Xiao, M., Dong, L., ... Li, W.-J. (2017). Meiothermus luteus sp. nov., a slightly thermophilic bacterium isolated from a hot spring [Journal Article]. *Int. J. Syst. Evol. Microbiol.*, *67*(8), 2910-2914. Retrieved from https://www.microbiologyresearch.org/content/journal/ijsem/10.1099/ijsem.0.002040 doi: 10.1099/ijsem.0.002040

Halpern, M., Shakèd, T., & Schumann, P. (2009). Brachymonas chironomi sp. nov., isolated from a chironomid egg mass, and emended description of the genus Brachymonas [Journal Article]. *International Journal of Systematic and Evolutionary Microbiology*, *59*(12), 3025-3029. Retrieved from https://www.microbiologyresearch.org/content/journal/ijsem/10.1099/ijs.0.007211-0 doi: https://doi.org/10.1099/ijs.0.007211-0

Hamilton, T. L., Peters, J. W., Skidmore, M. L., & Boyd, E. S. (2013). Molecular evidence for an active endogenous microbiome beneath glacial ice. *ISME J.*, *7*(7), 1402–1412. Retrieved from https://doi.org/10.1038/ismej.2013.31 doi: 10.1038/ismej.2013.31

Hanson, R. S., & Hanson, T. E. (1996). Methanotrophic bacteria. *Microbiol. Mol. Biol. Rev.*, *60*(2), 439–471. Retrieved from https://mmbr.asm.org/content/60/2/439

Henry, E. A., Devereux, R., Maki, J. S., Gilmour, C. C., Woese, C. R., Mandelco, L., ... Mitchell, R. (1994). Characterization of a new thermophilic sulfate-reducing bacterium. *Arch. Microbiol.*, *161*(1), 62–69. Retrieved from https://doi.org/10.1007/BF00248894 doi: 10.1007/BF00248894

Hiraishi, A., Sugiyama, J., & Shin, Y. K. (1995). *BRACHYMONAS DENITRIFICANS* GEN. NOV., SP. NOV., AN AEROBIC CHEMOORGANOTROPHIC BACTERIUM WHICH CONTAINS RHODOQUINONES, AND EVOLUTIONARY RELATIONSHIPS OF RHODOQUINONE PRODUCERS TO BACTERIAL SPECIES WITH VARIOUS QUINONE CLASSES. *J. Gen. Appl. Microbiol.*, *41*(2), 99-117. doi: 10.2323/jgam.41.99

Horibe, Y., & Craig, H. (1995). DH fractionation in the system methane-hydrogen-water. *Geochim. Cosmochim. Acta*, *59*(24), 5209–5217. doi: 10.1016/0016-7037(95)00391-6

Jeanpert, J., Iseppi, M., Adler, P., Genthon, P., Sevin, B., Thovert, J.-F., ... Join, J.-L. (2019). Fracture controlled permeability of ultramafic basement aquifers. inferences from the koniambo massif, new caledonia. *Eng. Geol.*, *256*, 67-83. Retrieved from https://www.sciencedirect.com/science/article/pii/S0013795218314224 doi: 10.1016/j.enggeo.2019.05.006

Kampbell, D., Wilson, J., & McInnes, D. (1998). DETERMINING DISSOLVED HYDROGEN, METHANE, AND VINYL CHLORIDE CONCENTRATIONS IN AQUEOUS SOLUTION ON A NANOMOLAR SCALE WITH THE BUBBLE STRIP METHOD. In *Proceedings of the 1998 conference on hazardous waste research* (p. 176-190).

Kelemen, P., Al Rajhi, A., Godard, M., Ildefonse, B., Köpke, J., MacLeod, C., ... Teagle, D. (2013). Scientific drilling and related research in the samail ophiolite, sultanate of Oman. *Scientific Drilling 2013 (2013), Nr. 15*, *2013*(15), 64–71. Retrieved from https://www.repo.uni-hannover.de/handle/123456789/1086

Kelemen, P., Matter, J., Teagle, D., Coggon, J., & the Oman Drilling Project Science Team. (2020). Proceedings of the oman drilling project. In *Proceedings of the oman drilling project* (p. All pages.). College Station, TX. doi: 10.14379/OmanDP.proc.2020

Kelemen, P. B., & Matter, J. (2008). In situ carbonation of peridotite for CO_2 storage. *Proc. Natl. Acad. Sci. U. S. A.*, *105*(45), 17295–17300. doi: 10.1073/pnas.0805794105

Kelemen, P. B., Matter, J., Streit, E. E., Rudge, J. F., Curry, W. B., & Blusztajn, J. (2011). Rates and mechanisms of mineral carbonation in peridotite: natural processes and recipes for enhanced, in situ CO_2 capture and storage. *Annu. Rev. Earth Planet. Sci.*, *39*, 545–576. doi: 10.1146/annurev-earth-092010-152509

Kelemen, P. B., Shimizu, N., & Salters, V. J. M. (1995, Jun). Extraction of mid-ocean-ridge basalt from the upwelling mantle by focused flow of melt in dunite channels. *Nature*, *375*(6534), 747–753. doi: 10.1038/375747a0

Kelley, D. S. (1996). Methane-rich fluids in the oceanic crust. *J. Geophys. Res.: Solid Earth*, *101*(B2), 2943–2962. doi: 10.1029/95JB02252

Kelley, D. S., & Früh-Green, G. L. (1999). Abiogenic methane in deep-seated mid-ocean ridge environments: Insights from stable isotope analyses. *J. Geophys. Res.: Solid Earth*, *104*(B5), 10439–10460. doi: 10.1029/1999JB900058

Klein, F., Grozeva, N. G., & Seewald, J. S. (2019). Abiotic methane synthesis and serpentinization in olivine-hosted fluid inclusions. *Proc. Natl. Acad. Sci. U. S. A.*, *116*(36), 17666–17672. Retrieved from https://www.pnas.org/content/116/36/17666 doi: 10.1073/pnas.1907871116

Kraus, E. A., Nothaft, D., Stamps, B. W., Rempfert, K. R., Ellison, E. T., Matter, J. M., ... Spear, J. R. (2021). Molecular Evidence for an Active Microbial Methane Cycle in Subsurface Serpentinite-Hosted Groundwaters in the Samail Ophiolite, Oman. *Appl. Environ. Microbiol.*, *87*(2). Retrieved from https://aem.asm.org/content/87/2/e02068-20 doi: 10.1128/AEM.02068-20

Labidi, J., Young, E., Giunta, T., Kohl, I., Seewald, J., Tang, H., ... Früh-Green, G. (2020). Methane thermometry in deep-sea hydrothermal systems: Evidence for re-ordering of doubly-substituted isotopologues during fluid cooling. *Geochim. Cosmochim. Acta*, *288*, 248 - 261. Retrieved from http://www.sciencedirect.com/science/article/pii/S0016703720305068 doi: 10.1016/j.gca.2020.08.013

Lang, S. Q., Früh-Green, G. L., Bernasconi, S. M., Brazelton, W. J., Schrenk, M. O., & McGonigle, J. M. (2018, Jan). Deeply-sourced formate fuels sulfate reducers but not methanogens at Lost City hydrothermal field. *Sci. Rep.*, *8*(1), 755. doi: 10.1038/s41598-017-19002-5

Leong, J. A. M., Howells, A. E., Robinson, K. J., Cox, A., Debes, R. V., Fecteau, K., ... Shock, E. (2020). Theoretical predictions vs environmental observations on serpentinization fluids: Lessons from the Samail ophiolite in Oman. *Earth and Space Sci. Open Archive*. doi: doi.org/10.1002/essoar.10504642.1

Leong, J. A. M., & Shock, E. L. (2020). Thermodynamic constraints on the geochemistry of low-temperature, continental, serpentinization-generated fluids. *Am. J. Sci.*, *320*(3), 185–235. doi: 10.2475/03.2020.01

Lin, X., Kennedy, D., Fredrickson, J., Bjornstad, B., & Konopka, A. (2012). Vertical stratification of subsurface microbial community composition across geological formations at the Hanford Site. *Environ. Microbiol.*, *14*(2), 414-425. Retrieved from https://sfamjournals.onlinelibrary.wiley.com/doi/abs/10.1111/j.1462-2920.2011.02659.x doi: 10.1111/j.1462-2920.2011.02659.x

Lods, G., Roubinet, D., Matter, J. M., Leprovost, R., & Gouze, P. (2020). Groundwater flow characterization of an ophiolitic hard-rock aquifer from cross-borehole multi-level hydraulic experiments. *Journal of Hydrology*, *589*, 125152. Retrieved from http://www.sciencedirect.com/science/article/pii/S0022169420306120 doi: https://doi.org/10.1016/j.jhydrol.2020.125152

Lovley, D. R., Chapelle, F. H., & Woodward, J. C. (1994, 07). Use of Dissolved H_2 Concentrations To Determine Distribution of Microbially Catalyzed Redox Reactions in Anoxic Groundwater. *Environ. Sci. Technol.*, *28*(7), 1205–1210. Retrieved from https://doi.org/10.1021/es00056a005 doi: 10.1021/es00056a005

Luef, B., Frischkorn, K. R., Wrighton, K. C., Holman, H.-Y. N., Birarda, G., Thomas, B. C., ... Banfield, J. F. (2015). Diverse uncultivated ultra-small bacterial cells in groundwater. *Nat. Commun.*, *6*(1), 6372. Retrieved from https://doi.org/10.1038/ncomms7372 doi: 10.1038/ncomms7372

Luther, G. W., Findlay, A., MacDonald, D., Owings, S., Hanson, T., Beinart, R., & Girguis, P. (2011). Thermodynamics and Kinetics of Sulfide Oxidation by Oxygen: A Look at Inorganically Controlled Reactions and Biologically Mediated Processes in the Environment. *Front. Microb.*, *2*, 62. Retrieved from https://www.frontiersin.org/article/10.3389/fmicb.2011.00062 doi: 10.3389/fmicb.2011.00062

Marques, J., Etiope, G., Neves, M., Carreira, P., Rocha, C., Vance, S., ... Suzuki, S. (2018). Linking serpentinization, hyperalkaline mineral waters and abiotic methane production in continental peridotites: an integrated hydrogeological-bio-geochemical model from the Cabeço de Vide CH_4-rich aquifer (Portugal). *Appl. Geochem.*, *96*, 287 - 301. Retrieved from http://www.sciencedirect.com/science/article/pii/S0883292718301987 doi: 10.1016/j.apgeochem.2018.07.011

Matter, J. M., Pezard, P. A., Moe, K., Henry, G., Paris, J., Brun, L., ... Coggon, J. A. (2018, December). Advanced downhole hydrogeophysical logging during Oman Drilling Project Phase 2 - Correlation of hydraulic and fluid properties. *AGU Fall Meeting Abstracts*.

Matter, J. M., Waber, H., Loew, S., & Matter, A. (2006). Recharge areas and geochemical evolution of groundwater in an alluvial aquifer system in the Sultanate of Oman. *Hydrogeol. J.*, *14*(1-2), 203–224. doi: 10.1007/s10040-004-0425-2

McCollom, T. M., & Bach, W. (2009). Thermodynamic constraints on hydrogen generation during serpentinization of ultramafic rocks. *Geochim. Cosmochim. Acta*, *73*(3), 856–875. doi: 10.1016/j.gca.2008.10.032

McCollom, T. M., & Seewald, J. S. (2003). Experimental constraints on the hydrothermal reactivity of organic acids and acid anions: I. Formic acid and formate. *Geochim. Cosmochim. Acta*, *67*(19), 3625 - 3644. Retrieved from `http://www.sciencedirect.com/science/article/pii/S0016703703001364` doi: 10.1016/S0016-7037(03)00136-4

Meyer-Dombard, D. R., Woycheese, K. M., Yargçoğlu, E. N., Cardace, D., Shock, E. L., Güleçal-Pektas, Y., & Temel, M. (2015). High pH microbial ecosystems in a newly discovered, ephemeral, serpentinizing fluid seep at Yanartaş (Chimera), Turkey. *Front. Microb.*, *5*, 723. Retrieved from `https://www.frontiersin.org/article/10.3389/fmicb.2014.00723` doi: 10.3389/fmicb.2014.00723

Milkov, A. V., & Etiope, G. (2018). Revised genetic diagrams for natural gases based on a global dataset of ¿20,000 samples. *Org. Geochem.*, *125*, 109–120. doi: 10.1016/j.orggeochem.2018.09.002

Miller, H. M., Matter, J. M., Kelemen, P., Ellison, E. T., Conrad, M. E., Fierer, N., ... Templeton, A. S. (2016). Modern water/rock reactions in Oman hyperalkaline peridotite aquifers and implications for microbial habitability. *Geochim. Cosmochim. Acta*, *179*, 217 - 241. Retrieved from `http://www.sciencedirect.com/science/article/pii/S0016703716300205` doi: 10.1016/j.gca.2016.01.033

Miller, H. M., Mayhew, L. E., Ellison, E. T., Kelemen, P., Kubo, M., & Templeton, A. S. (2017). Low temperature hydrogen production during experimental hydration of partially-serpentinized dunite. *Geochim. Cosmochim. Acta*, *209*, 161 - 183. Retrieved from `http://www.sciencedirect.com/science/article/pii/S0016703717302454` doi: 10.1016/j.gca.2017.04.022

Mitchell, P. (2011). Chemiosmotic coupling in oxidative and photosynthetic phosphorylation. *Biochim. Biophys. Acta - Bioenerg.*, *1807*(12), 1507 - 1538. Retrieved from `http://www.sciencedirect.com/science/article/pii/S0005272811002283` (Special Section: Peter Mitchell - 50th anniversary of the chemiosmotic theory) doi: 10.1016/j.bbabio.2011.09.018

Miura, M., Arai, S., & Mizukami, T. (2011). Raman spectroscopy of hydrous inclusions in olivine and orthopyroxene in ophiolitic harzburgite: Implications for elementary processes in serpentinization. *J. Mineral. Petrol. Sci.*, *advpub*, 1103030170-1103030170. doi: 10.2465/jmps.101021d

Morrill, P. L., Kuenen, J. G., Johnson, O. J., Suzuki, S., Rietze, A., Sessions, A. L., ... Nealson, K. H. (2013). Geochemistry and geobiology of a present-day serpentinization site in California: The Cedars. *Geochim. Cosmochim. Acta*, *109*, 222–240. doi: 10.1016/j.gca.2013.01.043

Mulkidjanian, A. Y., Dibrov, P., & Galperin, M. Y. (2008). The past and present of sodium energetics: May the sodium-motive force be with you. *Biochim. Biophys. Acta - Bioenerg.*, *1777*(7), 985 - 992. Retrieved from `http://www.sciencedirect.com/science/article/pii/S0005272808001266` (15th European Bioenergetics Conference 2008) doi: 10.1016/j.bbabio.2008.04.028

Neal, C., & Stanger, G. (1983). Hydrogen generation from mantle source rocks

in Oman. *Earth Planet. Sci. Lett.*, *66*, 315 - 320. Retrieved from http://www.sciencedirect.com/science/article/pii/0012821X83901449 doi: 10.1016/0012-821X(83)90144-9

Neal, C., & Stanger, G. (1985). Past and present serpentinisation of ultramafic rocks; an example from the Semail Ophiolite Nappe of Northern Oman. In *The chemistry of weathering* (pp. 249–275). Springer. doi: 10.1007/978-94-009-5333-8_15

Nealson, K. H., Inagaki, F., & Takai, K. (2005). Hydrogen-driven subsurface lithoautotrophic microbial ecosystems (SLiMEs): do they exist and why should we care? *Trends Microbiol.*, *13*(9), 405–410. doi: 10.1016/j.tim.2005.07.010

Nothaft, D. B., Templeton, A. S., Rhim, J. H., Wang, D. T., Labidi, J., Miller, H. M., ... The Oman Drilling Project Science Team (2020). Geochemical, biological and clumped isotopologue evidence for substantial microbial methane production under carbon limitation in serpentinites of the Samail Ophiolite, Oman. *Earth and Space Sci. Open Archive*. Retrieved from https://doi.org/10.1002/essoar.10504124.1 doi: 10.1002/essoar.10504124.1

Op den Camp, H. J. M., Islam, T., Stott, M. B., Harhangi, H. R., Hynes, A., Schouten, S., ... Dunfield, P. F. (2009). Environmental, genomic and taxonomic perspectives on methanotrophic Verrucomicrobia. *Environ. Microbiol. Rep.*, *1*(5), 293-306. Retrieved from https://onlinelibrary.wiley.com/doi/abs/10.1111/j.1758-2229.2009.00022.x doi: 10.1111/j.1758-2229.2009.00022.x

Paukert, A. (2014). *Mineral Carbonation in Mantle Peridotite of the Samail Ophiolite, Oman: Implications for permanent geological carbon dioxide capture and storage* (Doctoral dissertation, Columbia University). doi: 10.7916/D85M63WZ

Paukert, A. N., Matter, J. M., Kelemen, P. B., Shock, E. L., & Havig, J. R. (2012). Reaction path modeling of enhanced in situ CO_2 mineralization for carbon sequestration in the peridotite of the Samail Ophiolite, Sultanate of Oman. *Chem. Geol.*, *330*, 86–100. doi: 10.1016/j.chemgeo.2012.08.013

Paukert Vankeuren, A. N., Matter, J. M., Stute, M., & Kelemen, P. B. (2019). Multitracer determination of apparent groundwater ages in peridotite aquifers within the Samail ophiolite, Sultanate of Oman. *Earth Planet. Sci. Lett.*, *516*, 37–48. doi: 10.1016/j.epsl.2019.03.007

Postec, A., Quéméneur, M., Bes, M., Mei, N., Benaïssa, F., Payri, C., ... Erauso, G. (2015). Microbial diversity in a submarine carbonate edifice from the serpentinizing hydrothermal system of the Prony Bay (New Caledonia) over a 6-year period. *Front. Microb.*, *6*, 857. Retrieved from https://www.frontiersin.org/article/10.3389/fmicb.2015.00857 doi: 10.3389/fmicb.2015.00857

Prinzhofer, A. A., & Huc, A. Y. (1995). Genetic and post-genetic molecular and isotopic fractionations in natural gases. *Chem. Geol.*, *126*(3), 281 - 290. Retrieved from http://www.sciencedirect.com/science/article/pii/0009254195001239 (Processes of Natural Gas Formation) doi: 10.1016/0009-2541(95)00123-9

Quast, C., Pruesse, E., Gerken, J., Peplies, J., Yarza, P., Yilmaz, P., ... Glöckner, F. O. (2012, Nov). The SILVA ribosomal RNA gene database project: improved data processing and web-based tools. *Nucleic Acids Res.*, *41*(D1), D590–D596. doi: 10.1093/nar/gks1219

Raposo, P., Viver, T., Albuquerque, L., Froufe, H., Barroso, C., Egas, C., ... da Costa, M. S. (2019). Transfer of meiothermus chliarophilus (tenreiro et al.1995) nobre et al. 1996, meiothermus roseus ming et al. 2016, meiothermus terrae yu et al. 2014 and meiothermus timidus pires et al. 2005, to calidithermus gen. nov., as calidithermus chliarophilus comb. nov., calidithermus roseus comb. nov., calidithermus terrae comb. nov. and ca-

lidithermus timidus comb. nov., respectively, and emended description of the genus meiothermus [Journal Article]. *International Journal of Systematic and Evolutionary Microbiology*, *69*(4), 1060-1069. Retrieved from https://www.microbiologyresearch.org/content/journal/ijsem/10.1099/ijsem.0.003270 doi: https://doi.org/10.1099/ijsem.0.003270

Rempfert, K. R., Miller, H. M., Bompard, N., Nothaft, D., Matter, J. M., Kelemen, P., ... Templeton, A. S. (2017, February). Geological and geochemical controls on subsurface microbial life in the Samail Ophiolite, Oman. *Front. Microb.*, *8*(56), 1-21. doi: 10.3389/fmicb.2017.00056

Sabuda, M. C., Brazelton, W. J., Putman, L. I., McCollom, T. M., Hoehler, T. M., Kubo, M. D. Y., ... Schrenk, M. O. (2020). A dynamic microbial sulfur cycle in a serpentinizing continental ophiolite. *Environ. Microbiol.*, *22*(6), 2329-2345. Retrieved from https://sfamjournals.onlinelibrary.wiley.com/doi/abs/10.1111/1462-2920.15006 doi: 10.1111/1462-2920.15006

Schleheck, D., Weiss, M., Pitluck, S., Bruce, D., Land, M. L., Han, S., ... Thomas, T. (2011, 12). Complete genome sequence of Parvibaculum lavamentivorans type strain (DS-1(T)). *Standards in genomic sci.*, *5*(3), 298–310. Retrieved from https://pubmed.ncbi.nlm.nih.gov/22675581 doi: 10.4056/sigs.2215005

Segadelli, S., Vescovi, P., Ogata, K., Chelli, A., Zanini, A., Boschetti, T., ... Celico, F. (2017). A conceptual hydrogeological model of ophiolitic aquifers (serpentinised peridotite): The test example of Mt. Prinzera (Northern Italy). *Hydro. Process.*, *31*(5), 1058-1073. Retrieved from https://onlinelibrary.wiley.com/doi/abs/10.1002/hyp.11090 doi: doi.org/10.1002/hyp.11090

Sekiguchi, Y., Muramatsu, M., Imachi, H., Narihiro, T., Ohashi, A., Harada, H., ... Kamagata, Y. (2008). Thermodesulfovibrio aggregans sp. nov. and Thermodesulfovibrio thiophilus sp. nov., anaerobic, thermophilic, sulfate-reducing bacteria isolated from thermophilic methanogenic sludge, and emended description of the genus Thermodesulfovibrio [Journal Article]. *Int. J. Syst. Evol. Microbiol.*, *58*(11), 2541-2548. Retrieved from https://www.microbiologyresearch.org/content/journal/ijsem/10.1099/ijs.0.2008/000893-0 doi: 10.1099/ijs.0.2008/000893-0

Suzuki, S., Ishii, S., Hoshino, T., Rietze, A., Tenney, A., Morrill, P. L., ... Nealson, K. H. (2017). Unusual metabolic diversity of hyperalkaliphilic microbial communities associated with subterranean serpentinization at The Cedars. *ISME J.*, *11*(11), 2584–2598. Retrieved from https://doi.org/10.1038/ismej.2017.111 doi: 10.1038/ismej.2017.111

Suzuki, S., Ishii, S., Wu, A., Cheung, A., Tenney, A., Wanger, G., ... Nealson, K. H. (2013). Microbial diversity in The Cedars, an ultrabasic, ultrareducing, and low salinity serpentinizing ecosystem. *Proc. Natl. Acad. Sci. U. S. A.*, *110*(38), 15336–15341. Retrieved from https://www.pnas.org/content/110/38/15336 doi: 10.1073/pnas.1302426110

Suzuki, S., Kuenen, J. G., Schipper, K., van der Velde, S., Ishii, S., Wu, A., ... Nealson, K. H. (2014, May). Physiological and genomic features of highly alkaliphilic hydrogen-utilizing Betaproteobacteria from a continental serpentinizing site. *Nat. Commun.*, *5*, 3900. doi: 10.1038/ncomms4900

Takami, H., Noguchi, H., Takaki, Y., Uchiyama, I., Toyoda, A., Nishi, S., ... Takai, K. (2012). A deeply branching thermophilic bacterium with an ancient acetyl-CoA pathway dominates a subsurface ecosystem. *PloS one*, *7*(1), e30559–e30559. Retrieved from https://pubmed.ncbi.nlm.nih.gov/22303444 doi: 10.1371/journal.pone.0030559

Templeton, A. S., Ellison, E. T., Glombitza, C., Morono, Y., Rempfert, K. R., Zeigler, S., ... The Oman Drilling Project Science Team (this issue). Accessing the subsurface biosphere within rocks undergoing active low-temperature ser-

pentinization in the Samail Ophiolite (Oman Drilling Project). *J. Geophys. Res.: Biogeosci.*.

Terzer, S., Wassenaar, L. I., Araguás-Araguás, L. J., & Aggarwal, P. K. (2013). Global isoscapes for $\delta^{18}O$ and $\delta^{2}H$ in precipitation: improved prediction using regionalized climatic regression models. *Hydrol. Earth Syst. Sci.*, *17*(11), 4713–4728. Retrieved from `https://www.hydrol-earth-syst-sci.net/17/4713/2013/` doi: 10.5194/hess-17-4713-2013

Vacquand, C., Deville, E., Beaumont, V., Guyot, F., Sissmann, O., Pillot, D., ... Prinzhofer, A. (2018). Reduced gas seepages in ophiolitic complexes: evidences for multiple origins of the H_2-CH_4-N_2 gas mixtures. *Geochim. Cosmochim. Acta*, *223*, 437–461. doi: 10.1016/j.gca.2017.12.018

Waldron, S., Scott, E. M., & Soulsby, C. (2007). Stable Isotope Analysis Reveals Lower-Order River Dissolved Inorganic Carbon Pools Are Highly Dynamic. *Environ. Sci. Technol.*, *41*(17), 6156-6162. Retrieved from `https://doi.org/10.1021/es0706089` (PMID: 17937296) doi: 10.1021/es0706089

Wang, D. T., Reeves, E. P., McDermott, J. M., Seewald, J. S., & Ono, S. (2018). Clumped isotopologue constraints on the origin of methane at seafloor hot springs. *Geochim. Cosmochim. Acta*, *223*, 141–158. doi: 10.1016/j.gca.2017.11.030

Wang, Q., Garrity, G. M., Tiedje, J. M., & Cole, J. R. (2007). Naïve Bayesian Classifier for Rapid Assignment of rRNA Sequences into the New Bacterial Taxonomy. *Appl. Environ. Microbiol.*, *73*(16), 5261–5267. Retrieved from `https://aem.asm.org/content/73/16/5261` doi: 10.1128/AEM.00062-07

Weyhenmeyer, C. E., Burns, S. J., Waber, H. N., Macumber, P. G., & Matter, A. (2002). Isotope study of moisture sources, recharge areas, and groundwater flow paths within the eastern Batinah coastal plain, Sultanate of Oman. *Water Resources Research*, *38*(10). doi: 10.1029/2000WR000149

Woycheese, K. M., Meyer-Dombard, D. R., Cardace, D., Argayosa, A. M., & Arcilla, C. A. (2015). Out of the dark: transitional subsurface-to-surface microbial diversity in a terrestrial serpentinizing seep (Manleluag, Pangasinan, the Philippines). *Front. Microb.*, *6*, 44. doi: 10.3389/fmicb.2015.00044

Young, E., Kohl, I., Lollar, B. S., Etiope, G., Rumble Iii, D., Li, S., ... others (2017). The relative abundances of resolved $^{12}CH_2D_2$ and $^{13}CH_3D$ and mechanisms controlling isotopic bond ordering in abiotic and biotic methane gases. *Geochim. Cosmochim. Acta*, *203*, 235–264. doi: 10.1016/j.gca.2016.12.041

Zeebe, R. E., & Wolf-Gladrow, D. (2001). *CO_2 in seawater: equilibrium, kinetics, isotopes* (No. 65). Elsevier.

Supporting Information for Aqueous geochemical and microbial variation across discrete depth intervals in a peridotite aquifer assessed using a packer system in the Samail Ophiolite, Oman

Daniel B. Nothaft[a,*], Alexis S. Templeton[a,*], Eric S. Boyd[b], Juerg M. Matter[c], Martin Stute[d,e], Amelia N. Paukert Vankeuren[f], The Oman Drilling Project Science Team

[a] *Department of Geological Sciences, University of Colorado, Boulder, CO, USA*
[b] *Department of Microbiology & Immunology, Montana State University, Bozeman, MT*
[c] *National Oceanography Centre, University of Southampton, Southampton, UK*
[d] *Barnard College, New York, NY, USA*
[e] *Lamont-Doherty Earth Observatory, Columbia University, Palisades, NY, USA*
[f] *California State University, Sacramento, Sacramento, CA, USA*

Contents

List of Tables

List of Figures

*Corresponding authors
Email addresses: daniel.nothaft@colorado.edu (Daniel B. Nothaft), alexis.templeton@colorado.edu (Alexis S. Templeton)

S1. Supplementary 16S rRNA gene sequencing

Two 1 L autoclaved glass bottles were filled with drill foam/fluid that had surfaced after subsurface circulation during drilling of BA1A in 2017. The drilling foam and fluid was filtered through 0.22 μm polycarbonate filters at Colorado School of Mines. The drill foam/fluid samples totaled 1.5 L in volume and were split into two replicates, resulting in 0.75 L of foam/fluid filtered for each replicate. Nucleic acids concentrated onto the filters were extracted, amplified, and sequenced as described by Kraus et al. (2018). The drill foam/fluid samples (Figure S8) show very little taxonomic overlap with the fluids samples with packers (Main Text Figure 5).

In addition, a cell size fractionation experiment was performed for biomass filtering of BA1A in 2018. The sequential in-line filter housings described in the main text correspond to the three white cylinders near the bottom of Figure S2. Main Text Figure 5 shows the results of sequencing 0.22 μm pore-diameter filters only. Results of sequencing filters of all pore diameters are reported in (Figure S7).

S2. Tables

Table S1: Mixing extents based on Si, after Leong et al. (2020).

Sample ID	$\sum$Si/ $\left[\mu\text{mol} \cdot \text{L}^{-1}\right]$	Mixing extent / [% of $Mg^{2+} - HCO_3^-$ water]
BA1A_2018_55-66	1.97×10^2	65
BA1A_2018_100-400	4.49×10^1	15
BA1A_2019_0-30	3.33×10^2	110[a]
BA1A_2019_41-65	1.56×10^2	51
BA1A_2019_108-132	2.13×10^1	7.0
BA1D_2019_45-75	8.51	2.8
BA1D_2019_102-132	5.88	1.9

[a]BA1A_2019_0-30 has a calculated mixing extent > 100 % we performed these calculations using the same $Mg^{2+} - HCO_3^-$ end member as Leong et al. (2020), which had a $c_{\sum \text{Si}}$ of 303 μmol $\cdot$ kg. This sample should be considered representative of a typical $Mg^{2+} - HCO_3^-$ water.

S3. Figures

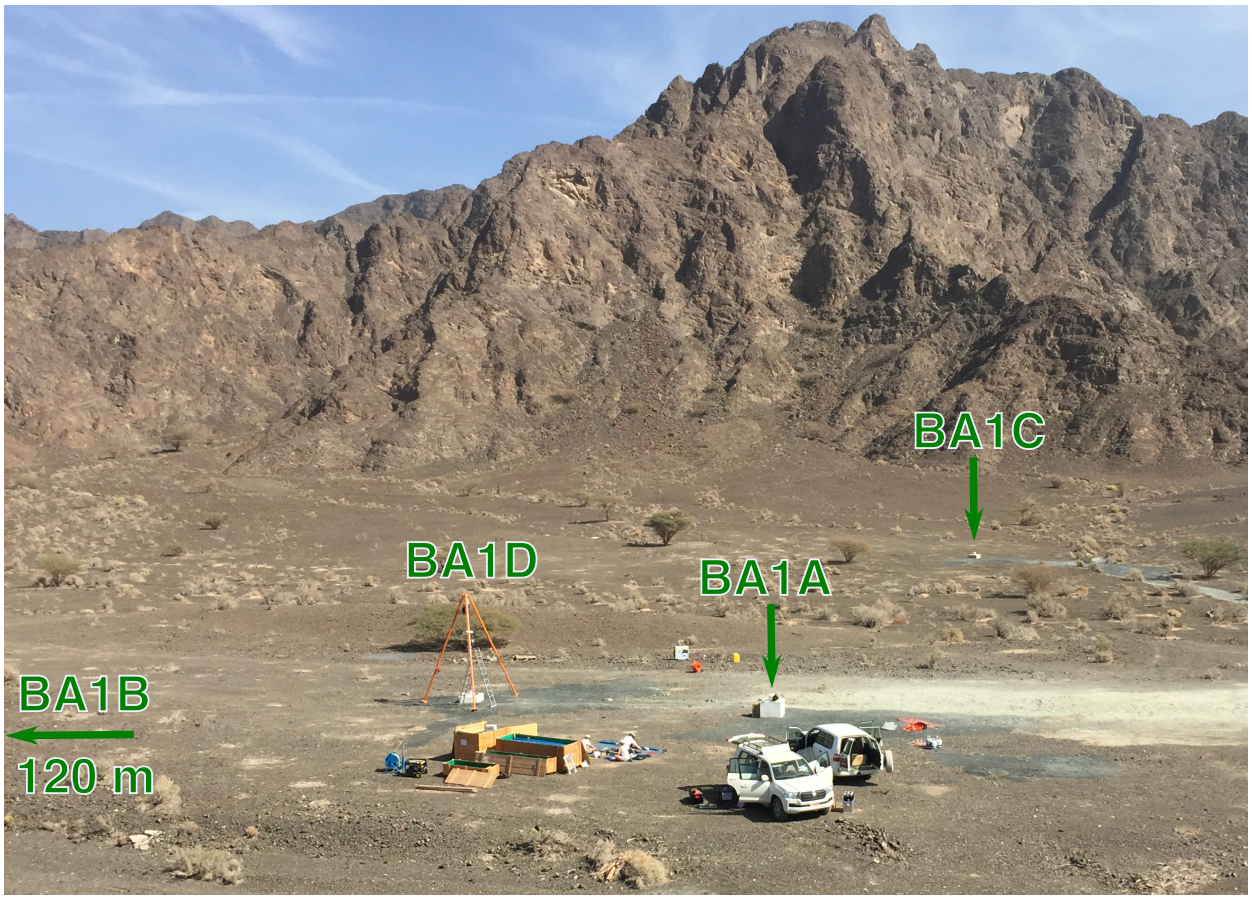

Figure S1: Packer installation at BA1D, January, 2019. The orange tripod, installed at BA1D in the photo, was used to suspend the packer assembly down hole. The wellhead of BA1A can be seen 15 m to the right of BA1D in the photo. The third rotary well at the BA1 site, BA1C, which collapsed shortly after drilling, is pictured in the background. The cored borehole, BA1B, is 120 m to the northwest, to the left of the frame.

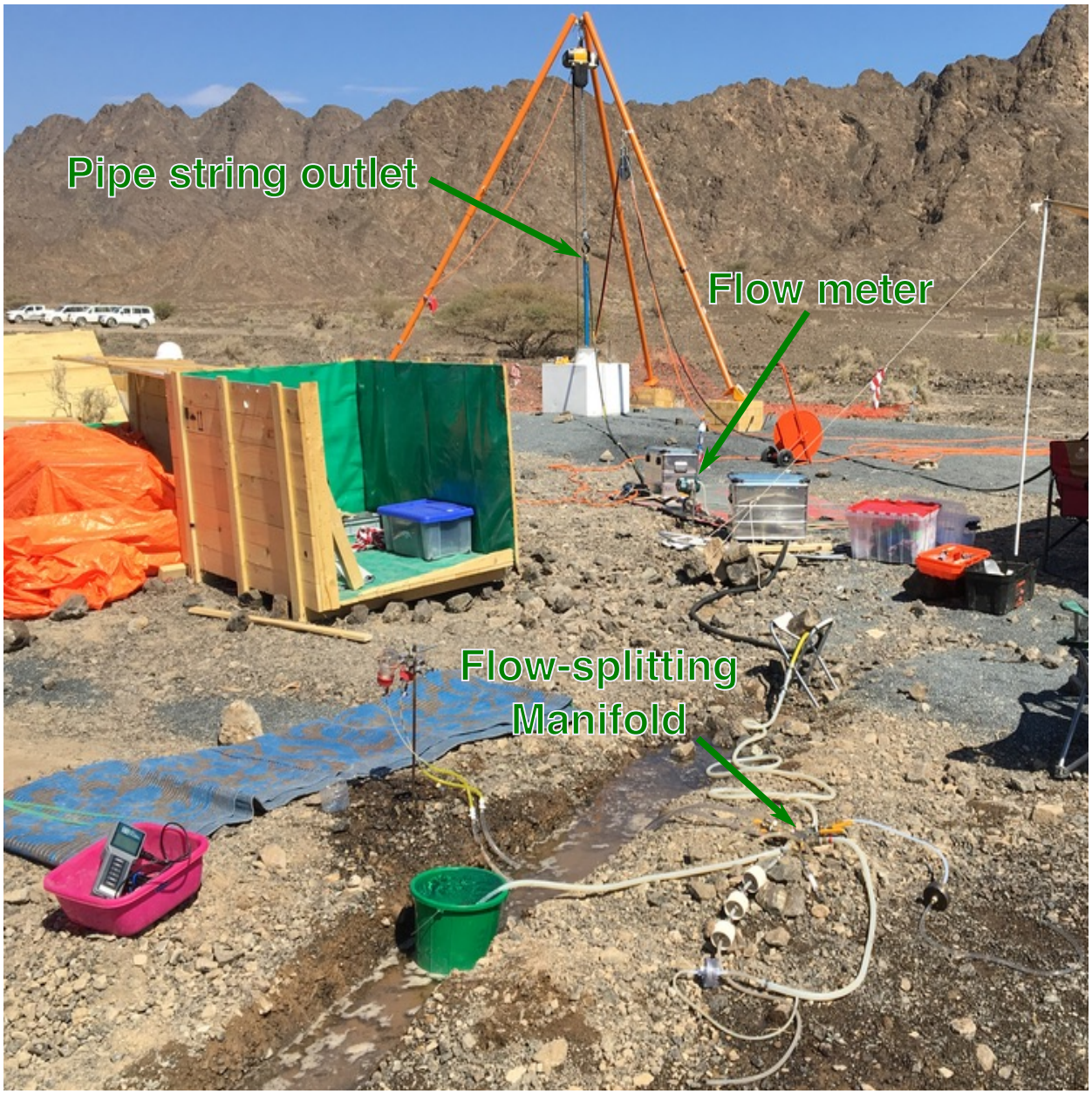

Figure S2: Fluid pumping and sampling at BA1A, February, 2019. Labeled arrows indicate the top of the pipe string, from which the pumped water flowed, the flow meter used for hydrologic pump tests, and the flow-splitting manifold used for fluid and biomass sampling.

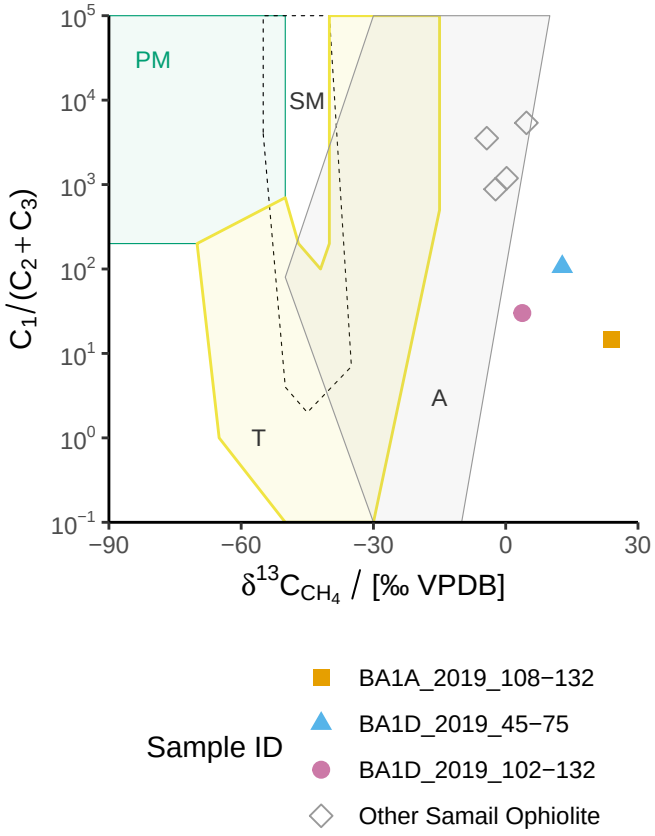

Figure S3: Plot of ratio of methane (C_1) to the sum of ethane (C_2) and propane (C_3) vs. $\delta^{13}C_{CH_4}$. Only analyses for which C_2 was above limit of quantitation are plotted. If C_3 was below limit of quantitation, its contribution to $C_1/(C_2+C_3)$ was assumed to be negligible, and therefore C_1/C_2 is plotted. Shaded fields of typical gas origin after Milkov and Etiope (2018). Contextual data from Samail Ophiolite from Nothaft et al., 2020; Etiope et al., 2015; Vacquand et al., 2018. *Abbreviations:* PM, primary microbial; SM, secondary microbial; T, thermogenic; A, abiotic.

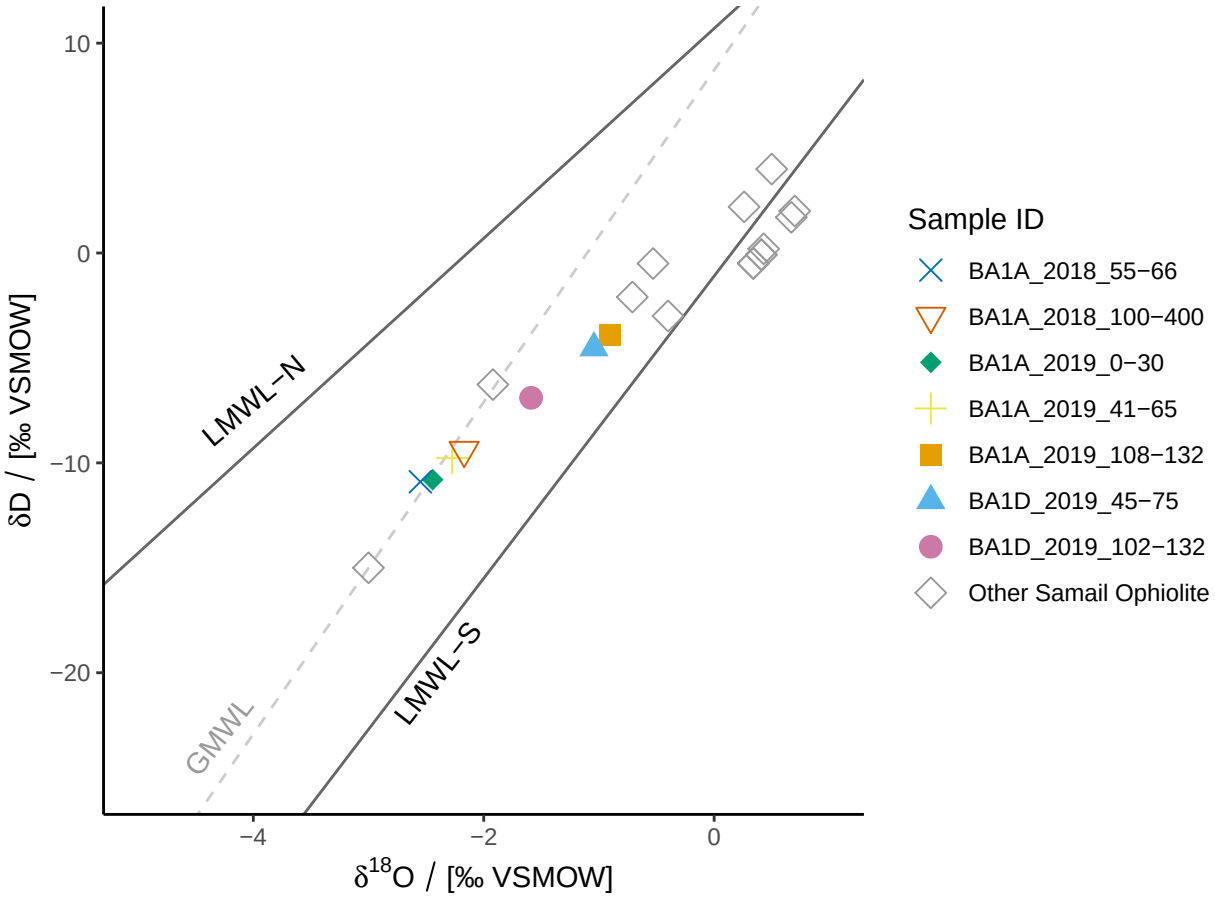

Figure S4: Plot of Oman groundwater stable isotopic compositions. Samples from 2012 were reported in Paukert Vankeuren et al. (2019). Samples from 2014 reported in Miller et al. (2016). Samples from 2018 (apart from BA1A) reported in Nothaft et al. (2020) *Abbreviations:* LMWL-N and LMWL-S, Oman local meteoric water lines derived from northern and southern sources, respectively (Weyhenmeyer et al., 2002); GMWL, global meteoric water line (Terzer et al., 2013).

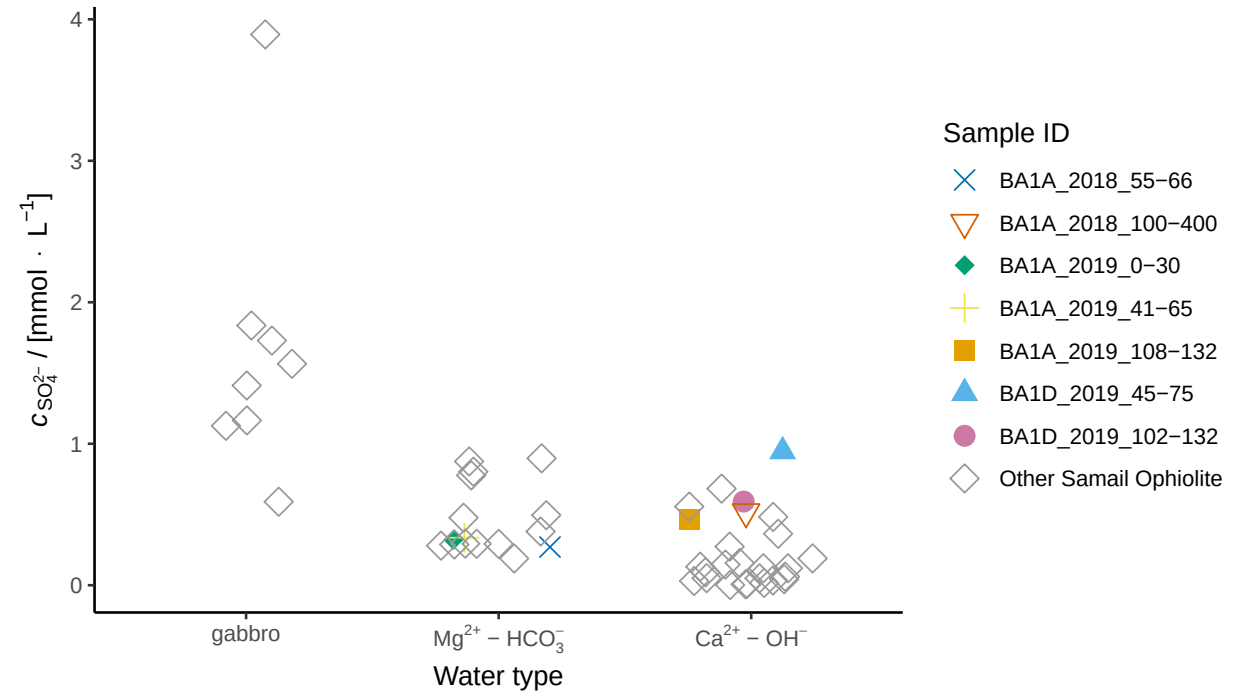

Figure S5: SO_4^{2-} concentrations in Samail Ophiolite wells. Data from Miller et al., 2016; Rempfert et al., 2017; Kraus et al., 2018; Nothaft et al., 2020.

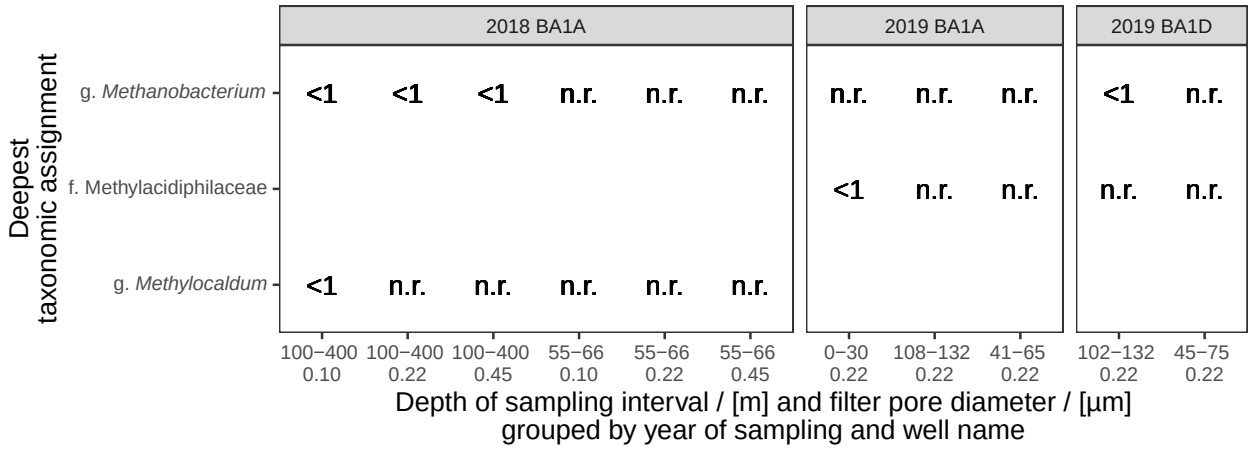

Figure S6: 16S rRNA gene read relative abundances of DNA extracted from filter-concentrated groundwaters from BA1A and BA1D affiliated with CH_4-cycling taxa. Read relative abundances are reported as percentages rounded to the ones place. Cases when a taxon was detected in a sample and was $< 1\,\%$ read relative abundance after rounding are labeled "< 1". Cases when no reads of a taxon were detected in a sample, but when that taxon was detected in 16S gene reads of other Oman samples obtained during the same sampling year, are labeled "n.r." Cases when no reads were detected in any Oman sample within the data set of a given year are blank."

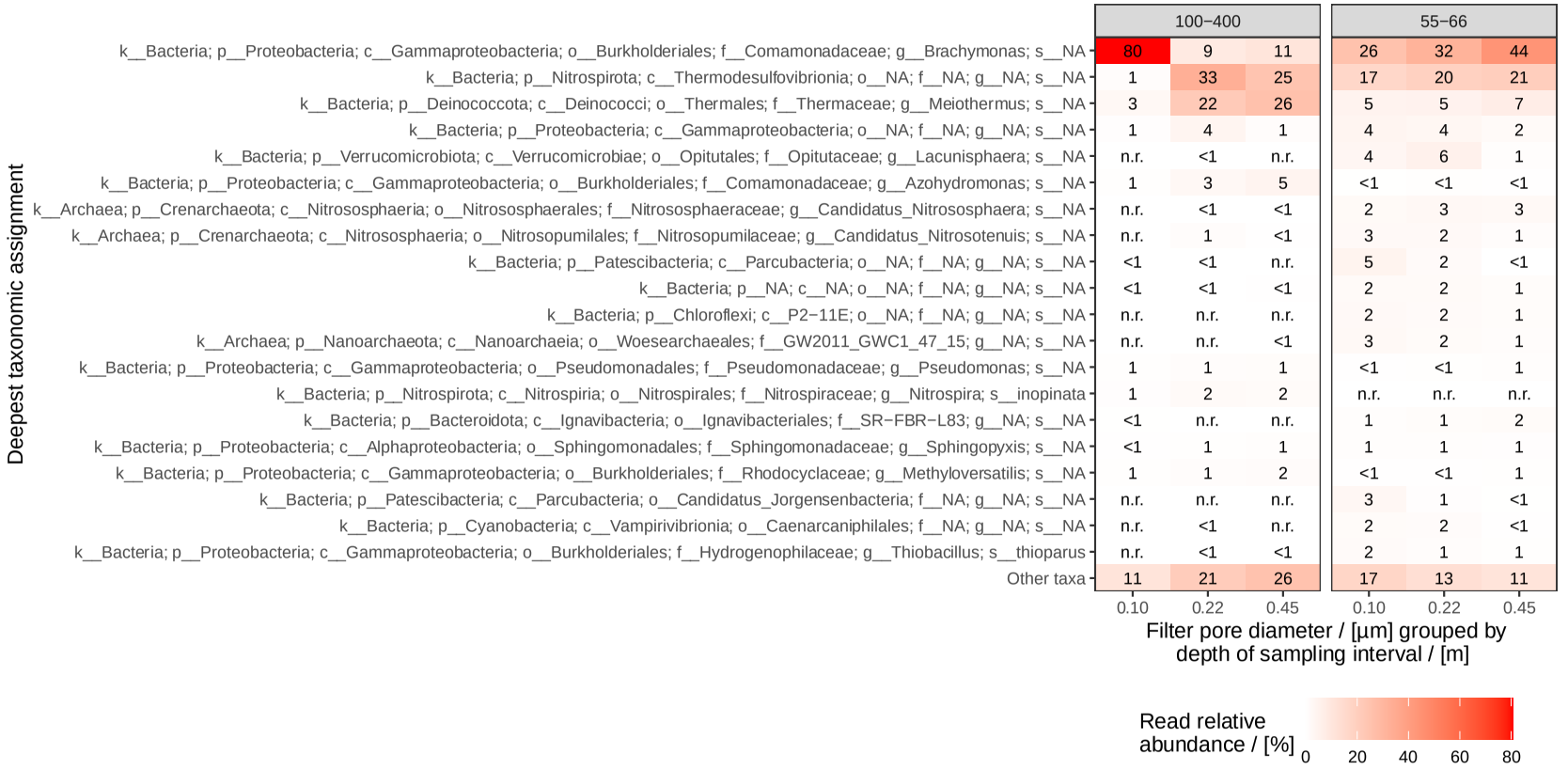

Figure S7: 16S rRNA gene read relative abundances of 20 most abundant taxonomic assignments in DNA extracted from groundwaters from which biomass was concentrated using inline filters of sequentially decreasing pore diameters from well BA1A in 2018. Read relative abundances are reported as percentages rounded to the ones place. Cases when a taxon was detected in a sample and was $< 1\,\%$ read relative abundance after rounding are labeled "< 1". Cases when no reads of a taxon were detected in a sample, but when that taxon was detected in 16S gene reads of other Oman samples obtained during the same sampling year, are labeled "n.r." Cases when no reads were detected in any Oman sample within the data set of a given year are blank."

Figure S8: 16S rRNA gene read relative abundances in of 20 most abundant taxonomic assignments in DNA and cDNA (from RNA) (Kraus et al., 2018) extracted from drill foam / fluid effluent from BA1A, acquired during drilling in 2017. Read relative abundances are reported as percentages rounded to the ones place. Cases when a taxon was detected in a sample and was $< 1\,\%$ read relative abundance after rounding are labeled "< 1". Cases when no reads of a taxon were detected in a sample, but when that taxon was detected in 16S gene reads of other Oman samples obtained during the same sampling year, are labeled "n.r." Cases when no reads were detected in any Oman sample within the data set of a given year are blank.

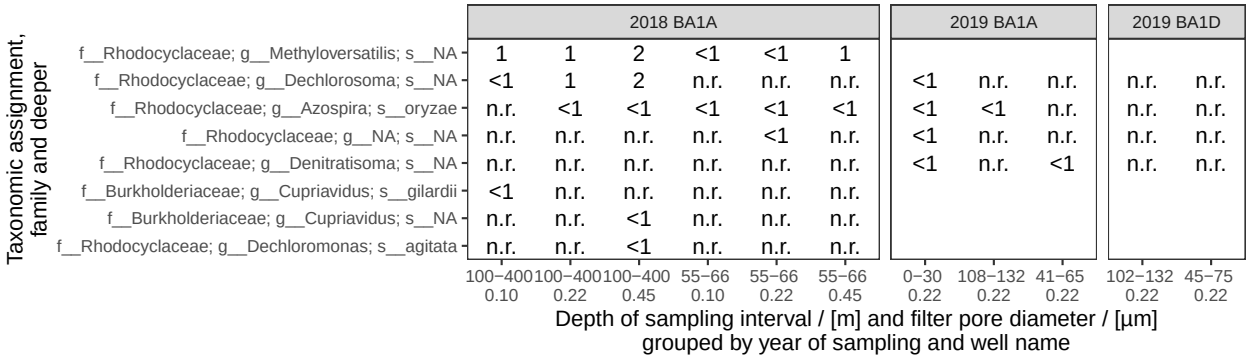

Figure S9: 16S rRNA gene read relative abundances of DNA extracted from filter-concentrated groundwaters from BA1A and BA1D affiliated with S-oxidizing taxa noted by Rempfert et al. (2017) (presented at family level and deeper). Read relative abundances are reported as percentages rounded to the ones place. Cases when a taxon was detected in a sample and was $< 1\,\%$ read relative abundance after rounding are labeled "< 1". Cases when no reads of a taxon were detected in a sample, but when that taxon was detected in 16S gene reads of other Oman samples obtained during the same sampling year, are labeled "n.r." Cases when no reads were detected in any Oman sample within the data set of a given year are blank."

S4. References

Etiope, G., Judas, J., Whiticar, M.. Occurrence of abiotic methane in the eastern United Arab Emirates ophiolite aquifer. Arabian J Geosci 2015;8(12):11345–11348. doi:10.1007/s12517-015-1975-4.

Kraus, E.A., Stamps, B.W., Rempfert, K.R., Nothaft, D.B., Boyd, E.S., Matter, J.M., Templeton, A.S., Spear, J.R.. Biological methane cycling in serpentinization-impacted fluids of the Samail ophiolite of Oman. AGU Fall Meeting Abstracts 2018;.

Leong, J., Howells, A., Robinson, K., Shock, E.. Diversity in the compositions of fluids hosted in continental serpentinizing systems. In: International Conference on Ophiolites and the Oceanic Lithosphere: Proceeding and Abstract Book. 2020. p. 130–131.

Milkov, A.V., Etiope, G.. Revised genetic diagrams for natural gases based on a global dataset of >20,000 samples. Org Geochem 2018;125:109–120. doi:10.1016/j.orggeochem.2018.09.002.

Miller, H.M., Matter, J.M., Kelemen, P., Ellison, E.T., Conrad, M.E., Fierer, N., Ruchala, T., Tominaga, M., Templeton, A.S.. Modern water/rock reactions in Oman hyperalkaline peridotite aquifers and implications for microbial habitability. Geochim Cosmochim Acta 2016;179:217 – 241. URL: http://www.sciencedirect.com/science/article/pii/S0016703716300205. doi:10.1016/j.gca.2016.01.033.

Nothaft, D.B., Templeton, A.S., Rhim, J.H., Wang, D.T., Labidi, J., Miller, H.M., Boyd, E.S., Matter, J.M., Ono, S., Young, E.D., Kopf, S.H., Kelemen, P.B., Conrad, M.E., The Oman Drilling Project Science Team, . Geochemical, biological and clumped isotopologue evidence for substantial microbial methane production under carbon limitation in serpentinites of the Samail Ophiolite, Oman. Earth and Space Sci Open Archive 2020;URL: https://doi.org/10.1002/essoar.10504124.1. doi:10.1002/essoar.10504124.1.

Paukert Vankeuren, A.N., Matter, J.M., Stute, M., Kelemen, P.B.. Multitracer determination of apparent groundwater ages in peridotite aquifers within the Samail ophiolite, Sultanate of Oman. Earth Planet Sci Lett 2019;516:37–48. doi:10.1016/j.epsl.2019.03.007.

Rempfert, K.R., Miller, H.M., Bompard, N., Nothaft, D., Matter, J.M., Kelemen, P., Fierer, N., Templeton, A.S.. Geological and geochemical controls on subsurface microbial life in the Samail Ophiolite, Oman. Front Microb 2017;8(56):1–21. doi:10.3389/fmicb.2017.00056.

70 Terzer, S., Wassenaar, L.I., Araguás-Araguás, L.J., Aggarwal, P.K.. Global isoscapes for δ^{18}O and δ^{2}H in precipitation:
71 improved prediction using regionalized climatic regression models. Hydrol Earth Syst Sci 2013;17(11):4713–4728. URL:
72 https://www.hydrol-earth-syst-sci.net/17/4713/2013/. doi:10.5194/hess-17-4713-2013.
73 Vacquand, C., Deville, E., Beaumont, V., Guyot, F., Sissmann, O., Pillot, D., Arcilla, C., Prinzhofer, A.. Reduced gas
74 seepages in ophiolitic complexes: evidences for multiple origins of the H_2-CH_4-N_2 gas mixtures. Geochim Cosmochim Acta
75 2018;223:437–461. doi:10.1016/j.gca.2017.12.018.
76 Weyhenmeyer, C.E., Burns, S.J., Waber, H.N., Macumber, P.G., Matter, A.. Isotope study of moisture sources, recharge
77 areas, and groundwater flow paths within the eastern Batinah coastal plain, Sultanate of Oman. Water Resources Research
78 2002;38(10). doi:10.1029/2000WR000149.